UCB-NE-5008

Reduction of TRU Toxicity in LWR-Spent Fuel by Reference ATW System with LBE-Cooled Transmuters

M. Cheon, J. Ahn, E. Greenspan, and P. L. Chambré

September 2004

Department of Nuclear Engineering
University of California
Berkeley, CA 94720
mgcheon@nuc.berkeley.edu, ahn@nuc.berkeley.edu

Table of Contents

1 Introduction

1.1 Review of ATW Concepts

Since the first nuclear power plant began its operation, spent nuclear fuel has been accumulating steadily in the U.S. as in other countries having nuclear power plants. The disposition of spent nuclear fuel continues to be an issue of national and international importance. In the U.S., a project is ongoing to develop the site at Yucca Mountain, Nevada for a geologic repository for spent nuclear fuel and high-level waste (HLW). Spent nuclear fuel from light-water reactors (LWRs) contains uranium, plutonium, other actinides, and fission products. Of the species in LWR spent fuel, some actinide and fission product isotopes have relatively long half-lives, and challenge to repository performance because it is difficult to predict performance hundreds of thousands of years in the future. The treatment of spent fuel to deal with these constituents could simplify some of the technical difficulties of geologic disposal. Such treatment can be considered as a technology options to enhance repository development. By removing and transmuting the plutonium, other transuranic constituents, and the long-lived fission products from spent nuclear fuel, several objectives can be achieved:

- By reducing the inventory of long-lived radionuclides in the repository, the period of time that the repository has to maintain integrity decreases.
- The potential for future recovery of plutonium from the repository for use in nuclear weapons is avoided.

- The energy content of the transuranics could instead be used in power reactors. The transuranics alone have an energy content equivalent to 25-30% of the energy released during the formation of the spent fuel.

One concept for reducing the amount and toxicity of this spent fuel is Accelerator-Driven Transmutation Technology (ADTT). Transmutation is a nuclear transformation that effectively converts one isotope into another. In terms of dealing with the problem components in spent nuclear fuel (roughly 1%), this involves fissioning the transuranic isotopes and converting the long-lived fission products into short-lived or stable isotopes. One of the most effective methods to achieve nuclear transmutation is through exposure of material to neutrons, either in a critical nuclear reactor or in an accelerator-driven subcritical nuclear system. In the latter, additional neutrons result from a beam of high-energy particles that collide with a dense, high-atomic-number target.

The lead ADTT concept in the U.S. is the Accelerator-driven Transmutation of Waste (ATW) system. The ATW system consists of three major technologies: (1) the chemistry processes that allow the spent fuel components to be separated, (2) the accelerator technology needed to provide a high power beam of charged particles, and (3) the target/blanket technology needed to transmute the long-lived hazards into stable or short-lived materials. Figure 1.1 shows components of an ATW system.

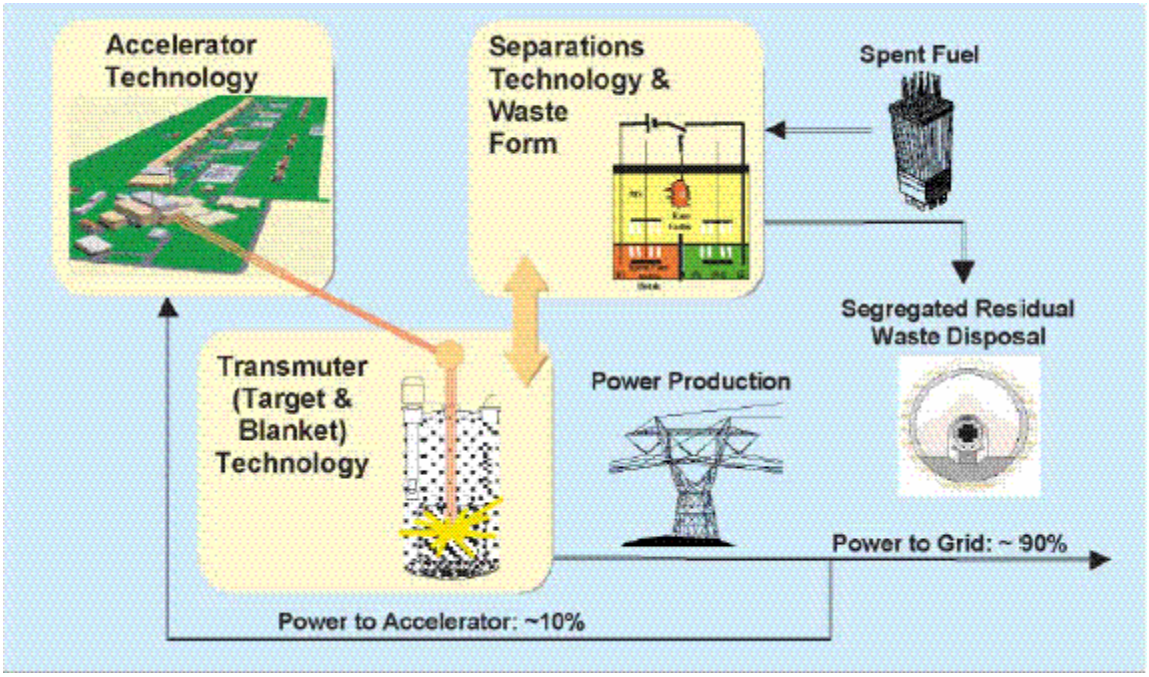

Figure 1.1 Components of an ATW system [1]

1.2 Reference ATW Plant in the Roadmap

A reference ATW plant was specified in a Roadmap for Developing ATW Technology [2] to process ~86,000 metric tons (MT) of initial heavy metal of spent nuclear fuel (SNF). This quantity will accumulate by year 2036 from existing U.S. nuclear power plants without license extensions. The ATW plant consists of several subcritical transmuters driven by linear accelerators, a separation facility, and a fuel fabrication facility. The reference ATW plant is designed to produce a net power of 6,720 MWt by fissioning the transuranics (TRU) taken from SNF during its life-time. It is also supposed to transmute long-lived fission products such as technetium and iodine into short-lived or stable isotopes as well as TRU.

According to the reference ATW plant deployment scenario specified in [2], after its complete operation, nearly all of the transuranics are supposed to be fissioned, most of the

technetium is expected to be converted to stable isotopes of ruthenium, and most of the iodine is expected to be transmuted to stable isotopes of xenon. The residual inventories of transuranics, technetium, and iodine from the last ATW unit are supposed to be of the order of a few hundred kilograms.

The reference ATW plant in the Roadmap is illustrated in Figure 1.2. It includes two large linear accelerators to provide proton beams to eight subcritical transmuters. The subcritical transmuters being considered in the reference ATW plant have a fast spectrum. To achieve a fast spectrum, a liquid metal is considered as a coolant.

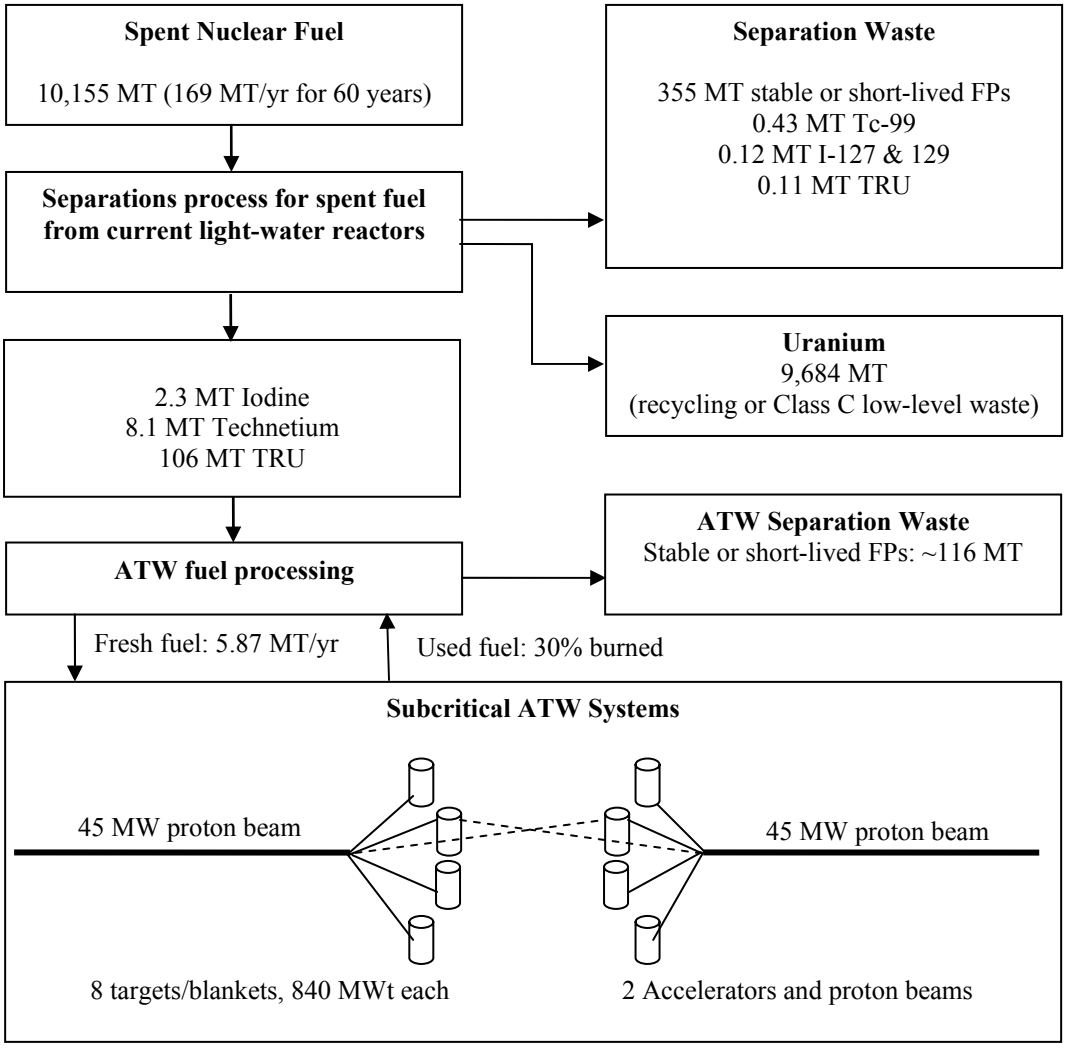

Figure 1.2 Reference ATW plant sized to process 10,155 MT of spent fuel [2]

1.3 Subcritical Transmuters of the Reference ATW Plant

For the subcritical transmuter of the reference ATW plant, many options can be considered. Options include a fast, epi-thermal, or thermal spectrum and a variety of coolant and fuel concepts. A fast spectrum was chosen for two reasons. First, nearly all actinides fission in a fast spectrum, giving maximum flexibility for the blend of fuel. In

contrast, a thermal spectrum renders some isotopes fissile and some fertile. Therefore, the system reactivity changes significantly during the burnup process, almost forcing the designer to use liquid fuel forms, which in turn raises significant safety issues. Second, the fast spectrum produces many excess neutrons that can be used to transmute iodine and technetium. To achieve a fast spectrum, a liquid metal is chosen as a coolant. Sodium was designated as the reference coolant because of an extensive international experience base. However, liquid lead-bismuth may offer significant advantages compared to sodium as both a spallation target and as a coolant, and is designated the preferred technology. As a fuel concept, metal fuel with high zirconium content, which has the ability to tolerate high burnup level is suggested. Structural material and cladding must be compatible with the chosen coolants. With sodium coolant, inconel and HT-9 are nearly ideal materials, with an excellent experience base that covers most conditions of interests. With liquid lead-bismuth, HT-9 can be used but inconel is not compatible with lead-bismuth, so alternate material would need to be demonstrated for beam entrance window [2].

1.4 Review of Available Codes

The evaluation of the performance characteristics of the transmutation system requires multi-cycle analysis of the reactor and fuel cycle facilities. There are several general purpose reactor analysis code systems that can perform multi-cycle burn-up analysis. Examples of such code systems are REBUS-3 developed at ANL [3], MOCUP developed at INEEL [4] and MONTEBURNS recently developed at LANL [5]. The latter two code systems use the ORIGEN 2 code developed by ORNL [6] for the burnup analysis. Some of the available code systems, such as REBUS-3, can automatically find the fuel composition

in the equilibrium cycle. However, applying the available design codes to study the time evolution of the fuel constituents in the ATW system requires significant effort and computer time. The effort is particularly demanding if the analysis is to include re-designing the core each cycle so as to get a given value of k_{eff} for the beginning of cycle (BOC) and another given value of k_{eff} at the end of cycle (EOC).

1.5 Objective of This Study

The purposes of the present work are (1) to develop a fuel cycle analysis tool for multi-cycle burnup analyses in a short time while accounting for the BOC and EOC k_{eff} constraints, and (2) to develop a tool that will couple the transmuting reactor performance analysis, out-of-core fuel cycle analysis and the repository performance analysis. The developed tool is intended primarily for scoping studies that compare different designs and mode of operation of ATW systems from the viewpoint of waste impact reduction.

The mathematical model developed is described in Chapter 2 & 3 and calculation procedures of single cycle and model benchmarking for a reference LBE-cooled transmuter are discussed in Chapter 4 & 5. Multi-cycle analysis of the LBE-cooled transmuter is described in Chapter 6. Reduction of TRU toxicity by the reference ATW transmuter is discussed in Chapter 7.

In this study, we consider a specific type of transmuter, a lead-bismuth eutectic (LBE) cooled, subcritical transmuter. We apply eight of these in the reference ATW plant and investigate its performance in the reduction of TRU in the SNF. Transmutation of long-lived fission products such as Tc and I have not been treated here.

After the review of the ATW deployment scenario, we numerically estimate the mass and the composition of the waste streams from the entire operation of the reference ATW plants, and compare them with those of the TRUs originally included in the light-water reactor spent fuels in terms of the radiotoxicity.

2 Reactor Model

We consider an ATW fuel cycle, shown in Figure 2.1. This ATW fuel cycle consists of an ATW-reactor, a partitioning plant, a fuel-fabrication facility, a makeup material storage, and a repository. Actinides are assumed to be recovered from the discharged fuel by the partitioning plant and passed through the fabrication plant before recycling. A *cycle* starts at the beginning of irradiation in the reactor. At the end of one irradiation period, the fraction, *f,* of the fuel in the core is discharged and partitioned. Recovered actinides are mixed with makeup materials (actinides and zirconium) and fabricated into fuel, which is returned to the reactor core. The initial composition of the fuel in the core for the next irradiation is determined. This is the point where one cycle ends. For sufficient transmutation of toxic actinides, this cycle needs to be repeated many times, as the numerical results from this study show.

The model is based on the following assumptions: (1) The reactor core is homogenized. (2) Partitioning of the discharged fuel and the fabrication are done instantaneously. Waste generation from the fabrication plant is neglected. (3) Only actinides are recovered, and all isotopes of element *e* are assumed to have the same recovery fraction, R_e. The recovery fraction is defined in Chapter 3. (4) The recharged fuel is mixed instantaneously and homogeneously with the fuel that stays in the core. (5) The reactor is operated at a constant power. (6) The fission products (FP) effect on the neutron multiplication factor k_{eff} is accounted for by considering a fictitious FP pair. (7) Effective one-group cross sections are used for reaction rate calculations. These are generated by MCNP [7] for the representative core composition and assumed to be constant within a cycle. (8) The total fuel volume in

the reactor is constant. (9) The actinides-to-Zr ratio is adjusted at each beginning of the cycle (BOC), so that the BOC k_{eff} will be 0.98. (10) The cycle terminates when k_{eff} drops to 0.92.

The present model can be divided into two parts: (1) determination of the fuel composition by nuclear reactions and decays in the reactor core and (2) determination of fuel composition after partitioning, fabrication, and reloading. In this chapter, we develop mathematical formulation for a mass flow model for a certain cycle.

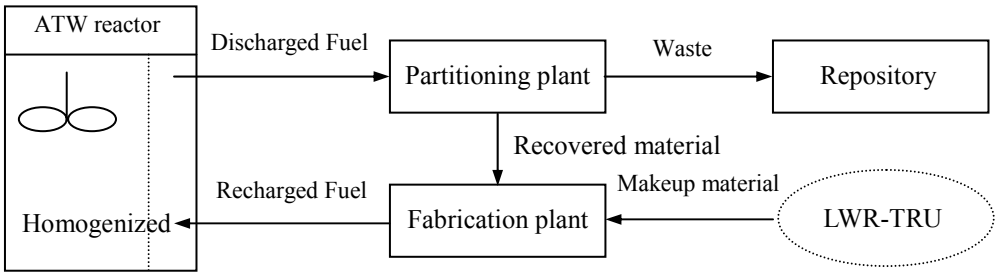

Figure 2.1 Simplified ATW fuel cycle

2.1 Transmutation Chain of Actinides

We develop a model for ^{234}U, ^{235}U, ^{236}U, ^{238}U, ^{237}Np, ^{238}Pu, ^{239}Pu, ^{240}Pu, ^{241}Pu, ^{242}Pu, ^{241}Am, ^{242m}Am, ^{243}Am, ^{242}Cm, ^{243}Cm, ^{244}Cm, ^{245}Cm, and ^{246}Cm. These nuclides are indexed by i from 1 to 18 in this order. Figure 2.2 shows the 18-nuclide chain considered in this work. The number in the parenthesis of each box shows the nuclide index, i. Three types of neutron reactions and four types of decay modes are considered to account for the mass change of a nuclide. If a nuclide captures a neutron, it turns into either a nuclide with the mass number greater by one, emitting a photon, or a nuclide with the mass number smaller

by one, emitting two neutrons. These are represented by vertical arrows in Figure 2.2. Upon neutron absorption, fission may also occur. The fission reaction is represented by letter "f" in Figure 2.2. A downward diagonal arrow represents an alpha decay, while a horizontal arrow indicates a beta (or EC) decay. The short-lived nuclides, ^{237}U, ^{239}U, ^{238}Np, ^{239}Np, ^{237}Pu, ^{243}Pu, ^{240}Am, ^{242}Am, ^{244}Am, and ^{241}Cm (6.75 day, 23.45 minute, 2.12 day, 2.36 day, 45.2 day, 4.96 hour, 50.8 hour, 16.0 hour, 10.1 hour, and 32.8 day [8], respectively), boxed by dotted lines in Figure 2.2, are not included in the present model. It is assumed that they decay into their daughter nuclides immediately.

Knowing the values, $\vec{N}^o$, at the beginning of the irradiation, the change of the numbers of atoms of nuclides, i = 1, 2, …, 18, in the fuel in the reactor core by the nuclear reactions and the radioactive decays shown in Figure 2.2 is expressed by

$$\frac{d\vec{N}(t)}{dt} = \mathbf{D}\vec{N}(t),\ 0 < t \le T \text{ , subject to } \vec{N}(0) = \vec{N}^o , \tag{2.1}$$

where $\vec{N}(t)$ is the vector whose elements express the number of atoms of each nuclide shown in Figure 2.2 during the irradiation period. The time t = 0 is the beginning of the irradiation time in the cycle, while $t = T$ is the end of the irradiation period in the same cycle. The value of the irradiation time length T is to be determined by numerically checking when the value of the neutron multiplication factor for the reactor core becomes equal to the specified lower-bound value (in this study it is assumed to be 0.92).

The matrix **D** represents the rate constants of the transmutation reactions in the nuclides with neutrons and for the radioactive decays, which are shown in Figure 2.2, and is formulated as

$$\mathbf{D} = (\mathbf{\Gamma}_p - \mathbf{\Gamma}_d)\phi(t) + (\mathbf{\Lambda}_p - \mathbf{\Lambda}_d), \tag{2.2}$$

where

$$\mathbf{\Gamma}_d = diag(\sigma_{a,1}, \sigma_{a,1}, \cdots, \sigma_{a,18}), \tag{2.3}$$

$$\mathbf{\Lambda}_d = diag(\lambda_1, \lambda_2, \cdots, \lambda_{18}), \tag{2.4}$$

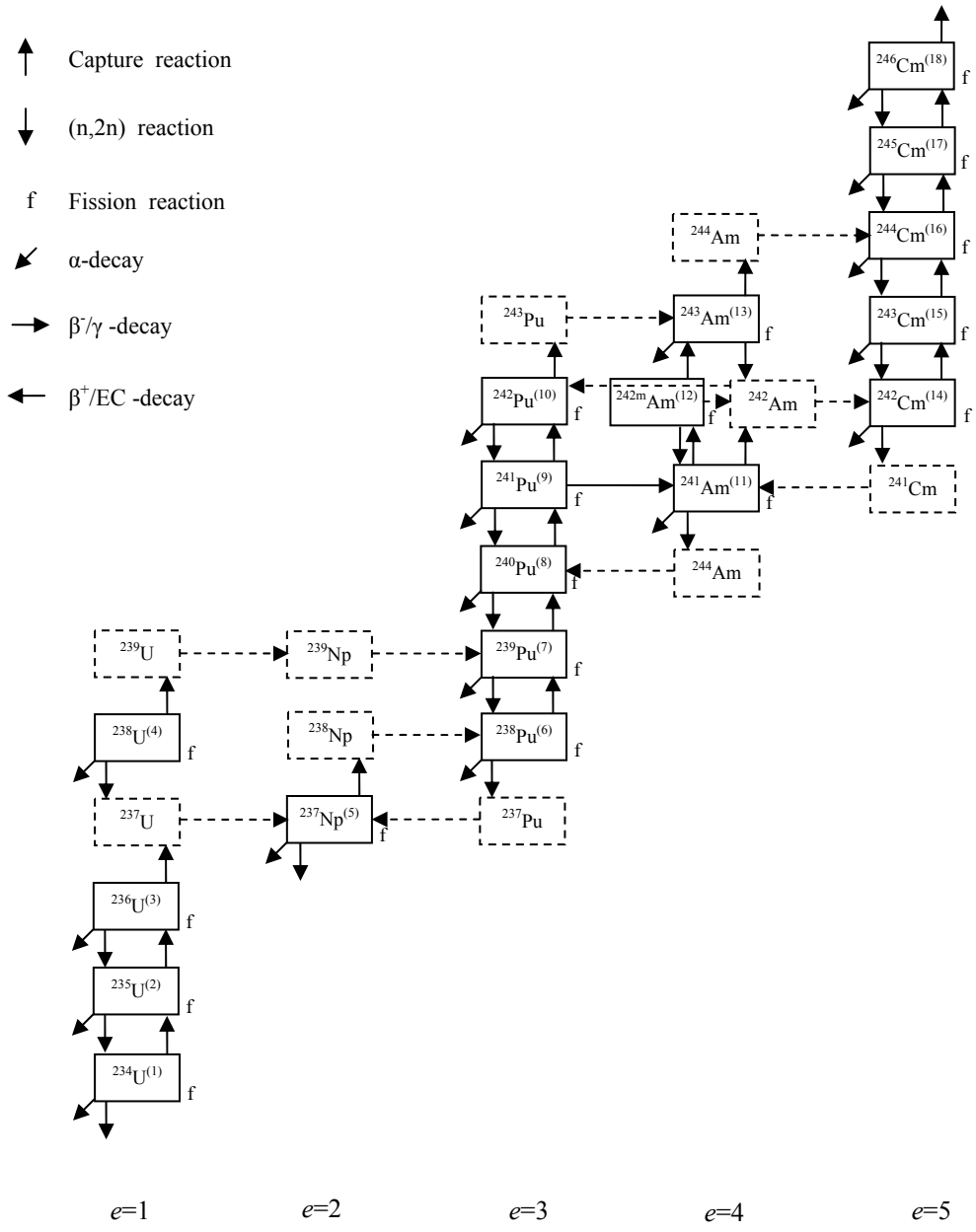

Figure 2.2 The 18-nuclide chain considered for this study

$$\Gamma_p \equiv \begin{bmatrix}
0 & \sigma_{2n,2} & 0 & 0 & 0 & 0 & 0 & 0 & 0 & 0 & 0 & 0 & 0 & 0 & 0 & 0 & 0 & 0 \\
\sigma_{\gamma,1} & 0 & \sigma_{2n,3} & 0 & 0 & 0 & 0 & 0 & 0 & 0 & 0 & 0 & 0 & 0 & 0 & 0 & 0 & 0 \\
0 & \sigma_{\gamma,2} & 0 & 0 & 0 & 0 & 0 & 0 & 0 & 0 & 0 & 0 & 0 & 0 & 0 & 0 & 0 & 0 \\
0 & 0 & 0 & 0 & 0 & 0 & 0 & 0 & 0 & 0 & 0 & 0 & 0 & 0 & 0 & 0 & 0 & 0 \\
0 & 0 & \sigma_{\gamma,3} & \sigma_{2n,4} & 0 & \sigma_{2n,6} & 0 & 0 & 0 & 0 & 0 & 0 & 0 & 0 & 0 & 0 & 0 & 0 \\
0 & 0 & 0 & 0 & \sigma_{\gamma,5} & 0 & \sigma_{2n,7} & 0 & 0 & 0 & 0 & 0 & 0 & 0 & 0 & 0 & 0 & 0 \\
0 & 0 & 0 & \sigma_{\gamma,4} & 0 & \sigma_{\gamma,6} & 0 & \sigma_{2n,8} & 0 & 0 & 0 & 0 & 0 & 0 & 0 & 0 & 0 & 0 \\
0 & 0 & 0 & 0 & 0 & 0 & \sigma_{\gamma,7} & 0 & \sigma_{2n,9} & 0 & \sigma_{2n,11} & 0 & 0 & 0 & 0 & 0 & 0 & 0 \\
0 & 0 & 0 & 0 & 0 & 0 & 0 & \sigma_{\gamma,8} & 0 & \sigma_{2n,10} & 0 & 0 & 0 & 0 & 0 & 0 & 0 & 0 \\
0 & 0 & 0 & 0 & 0 & 0 & 0 & 0 & \sigma_{\gamma,9} & 0 & 0.173\delta\sigma_{\gamma,11} & 0 & 0.173\sigma_{2n,13} & 0 & 0 & 0 & 0 & 0 \\
0 & 0 & 0 & 0 & 0 & 0 & 0 & 0 & 0 & 0 & 00 & \sigma_{2n,12} & 0 & \sigma_{2n,14} & 0 & 0 & 0 & 0 \\
0 & 0 & 0 & 0 & 0 & 0 & 0 & 0 & 0 & 0 & (1-\delta)\sigma_{\gamma,11} & 0 & 0 & 0 & 0 & 0 & 0 & 0 \\
0 & 0 & 0 & 0 & 0 & 0 & 0 & 0 & 0 & \sigma_{\gamma,10} & 0 & \sigma_{\gamma,12} & 0 & 0 & 0 & 0 & 0 & 0 \\
0 & 0 & 0 & 0 & 0 & 0 & 0 & 0 & 0 & 0 & 0.827\delta\sigma_{\gamma,11} & 0 & 0.827\sigma_{2n,13} & 0 & \sigma_{2n,15} & 0 & 0 & 0 \\
0 & 0 & 0 & 0 & 0 & 0 & 0 & 0 & 0 & 0 & 0 & 0 & 0 & \sigma_{\gamma,14} & 0 & \sigma_{2n,16} & 0 & 0 \\
0 & 0 & 0 & 0 & 0 & 0 & 0 & 0 & 0 & 0 & 0 & 0 & \sigma_{\gamma,13} & 0 & \sigma_{\gamma,15} & 0 & \sigma_{2n,17} & 0 \\
0 & 0 & 0 & 0 & 0 & 0 & 0 & 0 & 0 & 0 & 0 & 0 & 0 & 0 & 0 & \sigma_{\gamma,16} & 0 & \sigma_{2n,18} \\
0 & 0 & 0 & 0 & 0 & 0 & 0 & 0 & 0 & 0 & 0 & 0 & 0 & 0 & 0 & 0 & \sigma_{\gamma,17} & 0
\end{bmatrix}$$

and

$$\Lambda_p \equiv \begin{bmatrix}
0 & 0 & 0 & 0 & 0 & \lambda_{\alpha,6} & 0 & 0 & 0 & 0 & 0 & 0 & 0 & 0 & 0 & 0 & 0 & 0 \\
0 & 0 & 0 & 0 & 0 & 0 & \lambda_{\alpha,7} & 0 & 0 & 0 & 0 & 0 & 0 & 0 & 0 & 0 & 0 & 0 \\
0 & 0 & 0 & 0 & 0 & 0 & 0 & \lambda_{\alpha,8} & 0 & 0 & 0 & 0 & 0 & 0 & 0 & 0 & 0 & 0 \\
0 & 0 & 0 & 0 & 0 & 0 & 0 & 0 & 0 & \lambda_{\alpha,10} & 0 & 0 & 0 & 0 & 0 & 0 & 0 & 0 \\
0 & 0 & 0 & 0 & 0 & 0 & 0 & 0 & 0 & 0 & \lambda_{\alpha,11} & 0 & 0 & 0 & 0 & 0 & 0 & 0 \\
0 & 0 & 0 & 0 & 0 & 0 & 0 & 0 & 0 & 0 & 0 & 0 & 0 & \lambda_{\alpha,14} & 0 & 0 & 0 & 0 \\
0 & 0 & 0 & 0 & 0 & 0 & 0 & 0 & 0 & 0 & 0 & 0 & \lambda_{\alpha,13} & 0 & \lambda_{\alpha,15} & 0 & 0 & 0 \\
0 & 0 & 0 & 0 & 0 & 0 & 0 & 0 & 0 & 0 & 0 & 0 & 0 & 0 & 0 & \lambda_{\alpha,16} & 0 & 0 \\
0 & 0 & 0 & 0 & 0 & 0 & 0 & 0 & 0 & 0 & 0 & 0 & 0 & 0 & 0 & 0 & \lambda_{\alpha,17} & 0 \\
0 & 0 & 0 & 0 & 0 & 0 & 0 & 0 & 0 & 0 & 0 & 0.173\lambda_{\gamma,12} & 0 & 0 & 0 & 0 & 0 & \lambda_{\alpha,18} \\
0 & 0 & 0 & 0 & 0 & 0 & 0 & 0 & 0 & \lambda_{\beta,9} & 0 & 0 & 0 & 0 & 0 & 0 & 0 & 0 \\
0 & 0 & 0 & 0 & 0 & 0 & 0 & 0 & 0 & 0 & 0 & 0 & 0 & 0 & 0 & 0 & 0 & 0 \\
0 & 0 & 0 & 0 & 0 & 0 & 0 & 0 & 0 & 0 & 0 & 0 & 0 & 0 & 0 & 0 & 0 & 0 \\
0 & 0 & 0 & 0 & 0 & 0 & 0 & 0 & 0 & 0 & 0 & 0.827\lambda_{\gamma,12} & 0 & 0 & 0 & 0 & 0 & 0 \\
0 & 0 & 0 & 0 & 0 & 0 & 0 & 0 & 0 & 0 & 0 & 0 & 0 & 0 & 0 & 0 & 0 & 0 \\
0 & 0 & 0 & 0 & 0 & 0 & 0 & 0 & 0 & 0 & 0 & 0 & 0 & 0 & 0 & 0 & 0 & 0 \\
0 & 0 & 0 & 0 & 0 & 0 & 0 & 0 & 0 & 0 & 0 & 0 & 0 & 0 & 0 & 0 & 0 & 0 \\
0 & 0 & 0 & 0 & 0 & 0 & 0 & 0 & 0 & 0 & 0 & 0 & 0 & 0 & 0 & 0 & 0 & 0
\end{bmatrix}.$$

$\sigma_{a,i}$ is the effective one-group cross-section for nuclide *i,* and is equal to the sum of those for the fission, $\sigma_{f,i}$, the (n, 2n), $\sigma_{2n,i}$, and the capture reactions, $\sigma_{\gamma,i}$, i.e.,

$$\sigma_{a,i} = \sigma_{f,i} + \sigma_{2n,i} + \sigma_{\gamma,i} . \tag{2.5}$$

λ_i is the radioactive decay constant for nuclide *i*, and is equal to the sum of those for alpha and other emissions. The decay constant for alpha emission is denoted specifically as $\lambda_{\alpha,i}$ for nuclide *i.* In the nuclide-chain model shown in Figure 2.2, only the beta decay of Pu-241 is included; other EC, β+, or γ decays expressed by dashed horizontal arrows in Figure 2.2 have so short half-lives that they are combined with previous reactions.

The quantity δ (assumed to be 0.8 in this model) is the branching ratio for the capture reaction in ^{241}Am. With the probability of δ, an atom of ^{241}Am that has absorbed a neutron would be transmuted to an ^{242}Am atom in the ground state, whereas with 1-δ it would be transmuted to an ^{242m}Am atom in the meta-stable state. An ^{242}Am atom then decays to a ^{242}Cm atom with the probability of 0.827, while it decays to ^{242}Pu with the probability of 0.173.

The fuel consists of actinide nuclides as well as zirconium, which is included as the base matrix. It is assumed that the number of atoms of zirconium does not change by the neutron reaction. The rate of fission-product-pair generation by the fission of actinide atoms is expressed by

$$\frac{dN_F(t)}{dt} = \sum_i \sigma_{f,i}\phi(t)N_i(t), \;\; 0 < t \le T , \tag{2.6}$$

where $N_F(t)$ is the number of fission-product pairs at time t in the reactor, $\phi(t)$ is the time-dependent neutron flux. The time-dependent neutron flux is calculated from the expression,

$$\phi(t) = \frac{6.242 \times 10^{18} P}{\sum_i \gamma_i \sigma_{f,i} N_i(t)}, \tag{2.7}$$

where P is the power [MWt] of the ATW reactor, which is assumed to be constant, and $N_i(t)$ is the number of atoms of nuclide i at time t in the reactor. γ_i is the recoverable energy of nuclide i per fission, and is given by [9]

$$\gamma_i = 1.29927 \times 10^{-3} Z^2 A^{1/2} + 33.12 \text{ [MeV]}. \tag{2.8}$$

2.2 Multiplication Factor Formula

To simulate the fuel burnup in the reactor, the reactivity loss of fuel in a cycle is constrained in this model. The reactivity change of a reactor core can be expressed by multiplication factor.

The multiplication factor, k, characterizing the chain reaction is defined as [10]

$$k \equiv \frac{\text{Number of fission neutrons in one generation}}{\text{Number of fission neutrons in preceding generation}}. \tag{2.9}$$

The multiplication factor characterizing a finite system is usually referred to the effective multiplication factor denoted by k_{eff}. In a finite system, neutrons produced from the preceding generation by fission reactions are absorbed in the system or leaked out of the system. The absorbed neutrons in the system interact with materials consisting of the system and cause fission or capture reactions. Therefore, for a finite system, (2.9) can be modified as

$$k_{eff} \equiv \frac{\text{Number of fission neutrons in one generation}}{\text{Leakage} + \text{Number of neutrons absorbed in the system in preceding generation}}. \tag{2.10}$$

In MCNP, calculating k_{eff} consists of estimating the mean number of fission neutrons produced in one generation per fission neutron started. A generation is the life of a neutron from birth in fission to death by escape, parasitic capture, or absorption leading to fission. The computational equivalent of a fission generation in MCNP is a k_{eff} cycle; i.e., a cycle is a computed estimate of an actual fission generation. Processes such as (n,2n) and (n,3n) reactions are considered internal to a cycle and do not act as termination. Therefore, k_{eff} is formulated as [7]

$$k_{eff} = \frac{\int_V \int_0^\infty \int_E \int_\Omega \nu\Sigma_f \Phi(r,t,E,\Omega) dV dt dE d\Omega}{\int_V \int_0^\infty \int_E \int_\Omega \nabla \cdot J dV dt dE d\Omega + \int_V \int_0^\infty \int_E \int_\Omega (\Sigma_c + \Sigma_f + \Sigma_m)\Phi(r,t,E,\Omega) dV dt dE d\Omega}, \tag{2.11}$$

where the phase-space variables are t, E, and Ω for time, energy, direction, and implicitly r for position with incremental volume dV around r. The denominator is the loss rate, which is the sum of leakage, capture, fission, and multiplicity (n,xn) terms. The multiplicity term is:

$$\begin{aligned} &\int_V \int_0^\infty \int_E \int_\Omega \Sigma_m \Phi dV dt dE d\Omega \\ &= \int_V \int_0^\infty \int_E \int_\Omega \Sigma_{n,2n} \Phi dV dt dE d\Omega - 2\int_V \int_0^\infty \int_E \int_\Omega \Sigma_{n,2n} \Phi dV dt dE d\Omega \\ &+ \int_V \int_0^\infty \int_E \int_\Omega \Sigma_{n,3n} \Phi dV dt dE d\Omega - 3\int_V \int_0^\infty \int_E \int_\Omega \Sigma_{n,3n} \Phi dV dt dE d\Omega + \cdots. \end{aligned} \tag{2.12}$$

In this model, the effective multiplication factor is calculated by using the effective one-group cross section data obtained from MCNP, and thus its value is supposed to be the same with that estimated by MCNP for a certain fuel composition. The homogenized

reactor core modeled here is composed of actinides, fission products, zirconium, and structure materials. Therefore, the effective multiplication factor of the core is formulated as

$$k_{eff} = \frac{\sum_i \eta_i N_i \bar{\sigma}_{a,i} \bar{\phi}}{leakage + \left\{ \sum_i N_i \left(\bar{\sigma}_{a,i} - 2\bar{\sigma}_{2n,i}\right) + N_F\left(\bar{\sigma}_{a,F} - 2\bar{\sigma}_{2n,F}\right) + N_{Zr}\left(\bar{\sigma}_{a,Zr} - 2\bar{\sigma}_{2n,Zr}\right) + \sum_P N_P\left(\bar{\sigma}_{a,P} - 2\bar{\sigma}_{2n,P}\right) \right\} \bar{\phi}}, \quad (2.13)$$

where $$\eta_i \equiv \frac{\nu_i \bar{\sigma}_{i,f}}{\bar{\sigma}_{i,a}}, \qquad i=1,2,\cdots,18, \quad (2.14)$$

ν_i = the average number of neutrons produced per neutron-induced fission in nuclide i ,

$\bar{\sigma}_{F,a}$ = the absorption cross-section of a fictitious fission-product pair,

$\bar{\sigma}_{F,2n}$ = the effective one-group (n,2n) cross-section of a fictitious fission-product pair,

$\bar{\sigma}_{Zr,a}$ = the effective one-group absorption cross-section of zirconium,

$\bar{\sigma}_{Zr,2n}$ = the effective one-group (n,2n) cross-section of zirconium,

$\bar{\sigma}_{P,a}$ = the effective one-group absorption cross-section of an element, p, in the structure or the coolant of the reactor,

$\bar{\sigma}_{P,2n}$ = the effective one-group (n,2n) cross-section of an element, p, in the structure or the coolant of the reactor, and

$\bar{\phi}$ =the space, solid angle, time, and energy averaged neutron flux.

The numerator in (2.13) represents the number of neutrons generated by neutron-induced fission, while the denominator denotes the number of neutrons lost by absorption reactions and leakage. In the denominator, the neutron multiplicity term such as (n,2n) or

(n,3n) reaction is not treated as a termination as in MCNP but (n,3n) reaction rate is neglected due to its very small fraction compared to (n,2n) reaction rate. The leakage is the number of neutrons that leak out of the homogenized core. It is estimated from the MCNP calculated neutron balance.

2.3 Numerical Scheme

To solve (2.1) numerically, a predictor-corrector method was used [11]. This method uses two derivatives to improve the estimate of the slope for a certain interval-one at initial point and another at the end point. The two derivatives are averaged to obtain an improved estimate of the slope for the entire interval. To extrapolate linearly from the value at the beginning of an interval to the value at the end of the interval, the slope at the beginning point is used. However, the obtained value from the slope at the previous point is not the final answer, but an intermediate prediction. This intermediate value is called a predictor. It allows the calculation of an estimated slope at the end of the interval. Thus, the two slopes can be combined to obtain an average slope for the interval. This average slope is then used to extrapolate linearly from the previous value to the next value. The newly obtained value at the end point of the interval is called a corrector. If we apply this method to (2.1) for a discrete time step, $[t_j, t_{j+1}]$, (2.1) can be expressed as

$$\frac{\vec{N}_n^{(j+1)} - \vec{N}_n^{(j)}}{\Delta t_n^{(j)}} = \mathbf{D}_n^{(j)} \vec{N}_n^{(j)}, \quad \Delta t_n^{(j)} = t_{j+1} - t_j . \tag{2.15}$$

From this, a predictor distinguished with a superscript *prime* is obtained by

$$\vec{N}_n^{(j+1)'} = \vec{N}_n^{(j)} + \mathbf{D}_n^{(j)} \vec{N}_n^{(j)} \Delta t_n^{(j)}, \tag{2.16}$$

and then a corrector is expressed as

$$\vec{N}_n^{(j+1)} = \vec{N}_n^{(j)} + \frac{1}{2}[\mathbf{D}_n^{(j)}\vec{N}_n^{(j)} + \mathbf{D}_n^{(j+1)'}\vec{N}_n^{(j+1)'}]\Delta t_n^{(j)} . \tag{2.17}$$

The percent relative error, ε, is defined as

$$\varepsilon \equiv \frac{\text{current approximation - previous approximation}}{\text{current approximation}} 100\% . \tag{2.18}$$

The size of time interval can be determined based on that the absolute value of the relative error becomes less than a prescribed value for a certain time step. For I-nuclides, we obtain I-different estimates for the size of time interval. The smallest one is the choice for the next step.

2.4 Verification of Numerical Scheme for 2-Nuclide Chain

To check the numerical scheme developed for the calculation of the fuel composition change in the reactor, analytical solutions for a simplified two-nuclide chain consisting of ^{235}U and ^{236}U are obtained under the condition of a constant neutron flux. If we neglect the effect of α decay in two nuclides, the rate equation for ^{235}U (N_1) is

$$\frac{dN_1}{dt} = -\bar{\sigma}_{1,a}\phi N_1 + \bar{\sigma}_{2,2n}\phi N_2, \quad N_1(t=0) = N_1^o , \tag{2.19}$$

and the rate equation for ^{236}U (N_2) is

$$\frac{dN_2}{dt} = -\bar{\sigma}_{2,a}\phi N_2 + \bar{\sigma}_{1,\gamma}\phi N_1, \quad N_2(t=0) = N_2^o . \tag{2.20}$$

Using the Laplace transform method, we can get the solutions of (2.19) and (2.20) as follows:

$$N_1(t) = \frac{\overline{\sigma}_{2,a} N_1^o + \overline{\sigma}_{2,2n} N_2^o}{\alpha - \beta} \phi (e^{\alpha t} - e^{\beta t}) + \frac{N_1^o}{\alpha - \beta} (\alpha e^{\alpha t} - \beta e^{\beta t}) , \tag{2.21}$$

$$N_2(t) = \frac{\overline{\sigma}_{1,\gamma} N_1^o + \overline{\sigma}_{1,a} N_2^o}{\alpha - \beta} \phi (e^{\alpha t} - e^{\beta t}) + \frac{N_2^o}{\alpha - \beta} (\alpha e^{\alpha t} - \beta e^{\beta t}) , \tag{2.22}$$

where

$$\alpha \equiv \frac{-\phi(\overline{\sigma}_{1,a} + \overline{\sigma}_{2,a}) + \phi\sqrt{(\overline{\sigma}_{1,a} - \overline{\sigma}_{2,a})^2 + 4\overline{\sigma}_{1,\gamma}\overline{\sigma}_{2,2n}}}{2} , \tag{2.23}$$

$$\beta \equiv \frac{-\phi(\overline{\sigma}_{1,a} + \overline{\sigma}_{2,a}) - \phi\sqrt{(\overline{\sigma}_{1,a} - \overline{\sigma}_{2,a})^2 + 4\overline{\sigma}_{1,\gamma}\overline{\sigma}_{2,2n}}}{2} . \tag{2.24}$$

Table 2.1 shows the input data used for this comparison. To compare under the same condition, a constant value of the neutron flux was used for both. The percent relative error to determine the size of time step in the developed model was applied as 0.01%.

Table 2.1 Input Data for Comparison with Analytical Solution

Nuclide	σ_a [b]	σ_γ [b]	σ_{2n} [b]	N(t=0)
$N_1(^{235}U)$	5.5846E-1	5.58E-1	4.61E-4	2.2223E+27
$N_2(^{236}U)$	4.8633E-1	4.86E-1	3.25E-4	2.2223E+27

Figure 2.3 shows the results of the numerical and analytical solutions for 1-year irradiation time. Two results show a very good agreement with each other.

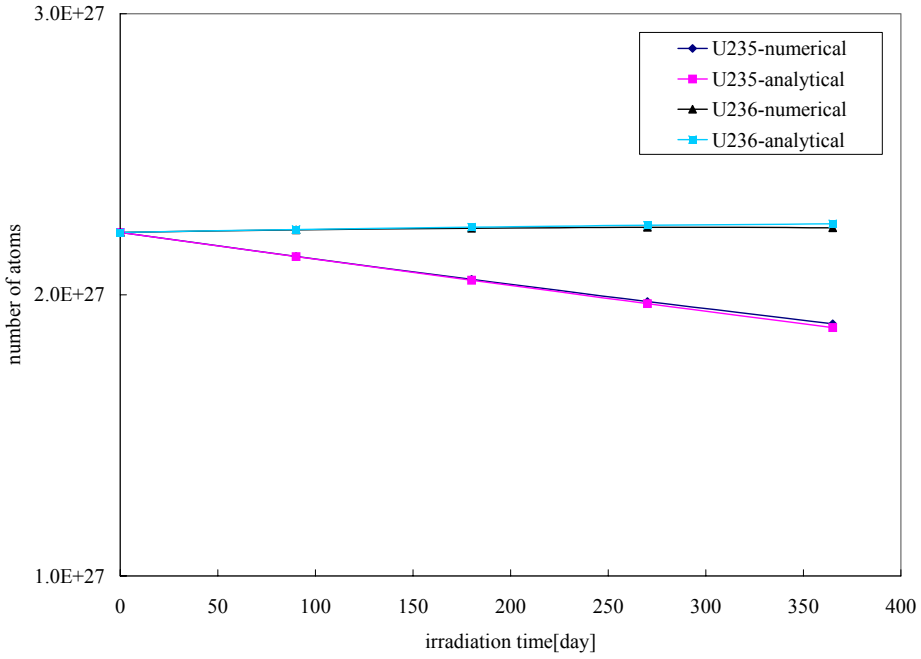

Figure 2.3 Results of the numerical and analytical solutions for 1-year irradiation time

3 Fuel Cycle Model

3.1 Fuel Discharge and Partitioning

After irradiation, the fraction *f* of the irradiated fuel is discharged. To describe the mass flow outside the reactor core, several vectors with different notations are introduced. The number of atoms of a nuclide discharged from the reactor core is expressed by the vector, $\vec{N}_{D,n}$, the number of atoms of a nuclide recovered from the discharged fuel by the vector, $\vec{N}_{R,n}$, the number of atoms of a nuclide in HLW by the vector, $\vec{N}_{W,n}$, the number of atoms of a nuclide in makeup material by the vector, $\vec{N}_{M,n}$, and the number of atoms of a nuclide in re-charged fuel by the vector, $\vec{N}_{C,n}$. $\vec{N}_{D,n}$ can be related to the vector, $\vec{N}_n(T_n^o + T_n)$ whose elements are the number of atoms of each nuclide in the reactor core at the end of the *n*-th cycle as

$$\vec{N}_{D,n} = f\vec{N}_n(T_n^o + T_n). \tag{3.1}$$

The volume of the discharged fuel, V_D, is expressed as

$$V_D = fV(T_n), \tag{3.2}$$

where $V(T_n)$ is the volume of the fuel in the reactor at the end of irradiation in the *n*-th cycle.

In the partitioning stage, actinide atoms in the discharged fuel are recovered for the next cycle. Actinides that are not recovered, together with zirconium and all fission products in the discharged fuel are solidified and sent to the repository as HLW. The recovery fraction of element *e*, R_e, in the partitioning is defined as the ratio of the number of atoms of element *e* recovered from the discharged fuel to that in the discharged fuel

before the partitioning occurs. Index *e* is used for numbering column in Figure 2.2. For example, all U isotopes are in column 1, all Np isotopes are in column 2, and so on. By mass balance,

$$\vec{N}_{D,n} = \vec{N}_{R,n} + \vec{N}_{W,n}. \tag{3.3}$$

We can write $\vec{N}_{R,n}$ and $\vec{N}_{W,n}$ as

$$\vec{N}_{R,n} = \mathbf{R}\vec{N}_{D,n} = \mathbf{R}f\vec{N}_n(T_n^o + T_n), \tag{3.4}$$

$$\vec{N}_{W,n} = (\mathbf{I} - \mathbf{R})\vec{N}_{D,n}, \tag{3.5}$$

where **I** is the unit matrix and **R** is the recovery fraction matrix. Elements of matrix **R** are all zero except for the diagonal elements. The diagonal elements are equal to the recovery fractions of corresponding elements. For example, the fifth diagonal element is equal to R_{Np}, which is the recovery fraction of ^{237}Np at the partitioning. By the assumption made at the beginning of this section, the isotopes of the same element have the same recovery fraction. For example, the first to the fourth diagonal elements correspond to the U isotopes in Figure 2.2. Therefore, these diagonal elements have the same value, R_U. The recovery fraction for element *e* must be in the range $0 \le R_e < 1$.

3.2 Determination of Makeup Fuel

In the fuel-fabrication facility, the recovered material inventory represented by the vector $\vec{N}_{R,n}$ is mixed with the makeup material inventory which is described by the vector, $\vec{N}_{M,n}$. A fuel with $\vec{N}_{C,n}$ is fabricated, and loaded into the reactor core. By mass balance,

$$\vec{N}_{C,n} = \vec{N}_{R,n} + \vec{N}_{M,n}. \tag{3.6}$$

By the volume constraint of this system, the volume, V_o , of the homogenized fuel at the beginning of each cycle should be kept constant through all cycles and thus, the volume, $V_{C,n}$, of the recharged fuel at the *n*-th cycle is determined as

$$V_{C,n} = V_o - V(T_n) + V_{D,n} . \tag{3.7}$$

$V_{C,n}$ can also be expressed in terms of the recovered material volume and the makeup material volume as

$$V_{C,n} = V_{R,n} + V_{M,n} , \tag{3.8}$$

where $V_{R,n}$ is the volume of the recovered material, and $V_{M,n}$ is that of the makeup material. $V_{R,n}$ is calculated from

$$V_{R,n} = \vec{\mu}^T \cdot \vec{N}_{R,n} , \tag{3.9}$$

where the elements of the vector, $\vec{\mu}$, are the reciprocals of the atomic density of nuclide *i*, and $\vec{\mu}^T$ is expressed as $\vec{\mu}^T = \{\rho_1^{-1}, \rho_2^{-1}, \rho_3^{-1}, ..., \rho_{18}^{-1}\}$.

The volume of makeup material, $V_{M,n}$, is the sum of the volume of actinides and that of zirconium. We set the volume fraction of actinides in the makeup material as ω. Then, the volume of actinides in the makeup material is $\omega V_{M,n}$. We determine ω in such a way that the recharged fuel has a sufficiently high actinide content so that the whole core at the beginning of the next irradiation period has a k_{eff} value of 0.98. The makeup material consists of actinides and zirconium taken from LWR-spent fuel. The atomic fraction, x_i, of actinide nuclide *i* in the makeup material is assumed to be constant. Then,

$$\omega V_{M,n} = N_{tot,M,n} \sum_i \frac{x_i}{\rho_i}, \quad 0 \le \omega \le 1 . \tag{3.10}$$

The total number of atoms, $N_{tot,M,n}$, of actinides in the makeup material at the n-th cycle and the number, $N_{i,M,n}$, of atoms of an actinide nuclide i in the makeup material are related by

$$N_{tot,M,n} \equiv \sum_i N_{i,M,n} \quad \text{and} \quad N_{i,M,n} = x_i N_{tot,M,n} . \tag{3.11}$$

The volume of zirconium in the makeup material, $(1-\omega)V_{M,n}$, can be written as

$$(1-\omega)V_{M,n} = \frac{N_{Zr,M,n}}{\rho_{Zr}}, \tag{3.12}$$

where ρ_{Zr} is the atomic density of zirconium.

The number of fuel atoms at the beginning of the (n+1)-st cycle is determined by summing the fuel remaining in the reactor core and the recharged fuel and thus

$$\vec{N}^{o}_{n+1} = (1-f)\vec{N}_n(T_n^o + T_n) + f\mathbf{R}\vec{N}_n(T_n^o + T_n) + \vec{N}_{M,n} \tag{3.13}$$

obtained by substituting (3.4) into (3.6). The vector $\vec{N}_{M,n}$ is yet to be determined. For this, the aforementioned k_{eff} constraints and the characteristics of actinide taken from the LWR-spent fuel are used. The value of k_{eff} of the reactor at the beginning of each irradiation period is set to be 0.98. Then, at the beginning of the (n+1)-st cycle, (2.13) must satisfy

$$\frac{\sum_i \eta_i N^o_{i,n+1}\overline{\sigma}_{i,a}}{\xi + \sum_i N^o_{i,n+1}(\overline{\sigma}_{i,a} - 2\overline{\sigma}_{i,2n}) + N^o_{F,n+1}(\overline{\sigma}_{F,a} - 2\overline{\sigma}_{F,2n}) + N^o_{Zr,n+1}(\overline{\sigma}_{Zr,a} - 2\overline{\sigma}_{Zr,2n}) + \sum_P N_P(\overline{\sigma}_{P,a} - 2\overline{\sigma}_{P,2n})} = 0.98$$

. (3.14)

The left side expresses the k_{eff} at the beginning of the (n+1)-st cycle. By (3.13) and (3.11), the number of atoms of an actinide i in the reactor at the (n+1)-st cycle is written as

$$N^o_{i,n+1} = (1-f)N_{i,n}(T^o_n + T_n) + fR_e N_{i,n}(T^o_n + T_n) + x_i N_{tot,M,n}. \tag{3.15}$$

The number of atoms of fission-product pairs in the reactor at the (n+1)-st cycle is written as

$$N^o_{F,n+1} = (1-f)N_{F,n}(T^o_n + T_n). \tag{3.16}$$

Using (3.10) and (3.12), the number of atoms of zirconium in the reactor at the beginning of the (n+1)-st cycle is given by

$$N^o_{Zr,n+1} = (1-f)N_{Zr,n}(T^o_n + T_n) + N_{Zr,M,n}$$

$$= (1-f)N_{Zr,n}(T^o_n + T_n) + \rho_{Zr}V_{M,n} - \rho_{Zr}N_{tot,M,n}\sum_i \frac{x_i}{\rho_i}. \tag{3.17}$$

Substituting (3.15), (3.16), and (3.17) into (3.14) yields an equation for $N_{tot,M,n}$. The value of $N_{tot,M,n}$ is obtained by solving that equation. By (3.10-2.34) and (3.11-2.35), the volume fraction, ω, of actinides in the makeup material at the n-th cycle and the number, $N_{i,M,n}$, of atoms of an actinide nuclide i can be determined. Once $N_{i,M,n}$ is known, $\vec{N}_{M,n}$ is determined also. The number, $N_{Zr,M,n}$, of atoms of zirconium in the makeup material at the n-th cycle is obtained by (3.12).

3.3 Flow Chart for Code Programming

To carry out ATW fuel cycle simulation on a computer, a computational procedure based on Chapters 2 and 3 was developed. Figure 2.4 shows a flow chart for code

programming. This algorithm starts fuel burnup calculation by reading input data such as material properties and neutronics of homogenized reactor core. Neutronics of homogenized reactor core estimated by MCNP are used. As the numerical solution for fuel burnup calculation, a predictor-corrector method is implemented. After fuel burnup calculation for a time step, the multiplication factor, k_{eff} , is estimated at the end of the time step. Then, the estimated k_{eff} is compared to the lower bound of its value, here 0.92. If the estimated k_{eff} is greater than 0.92, fuel burnup calculation is performed for the next time step until it satisfies the condition, $k_{eff} \leq 0.92$. When k_{eff} satisfies the condition, burnup calculation stops and the composition vector of discharged fuel is determined from the composition vector of the irradiated fuel multiplied by the discharge fraction (f). As the next step, by multiplying the composition vector of the discharged fuel by the recovery matrix (**R**), the composition vector of the recovered fuel is obtained and the composition vector of waste is subsequently determined. The mass and the composition of makeup material are determined such that k_{eff} of the recharged reactor core at BOC gives the upper bound of k_{eff}, here 0.98. The summation of the composition vectors of the recovered and the makeup materials results in the composition vector of the newly charged fuel. By determining the composition vector of the recharged core, the calculation of the first cycle ends. For multi-cycles, the whole procedure is repeated.

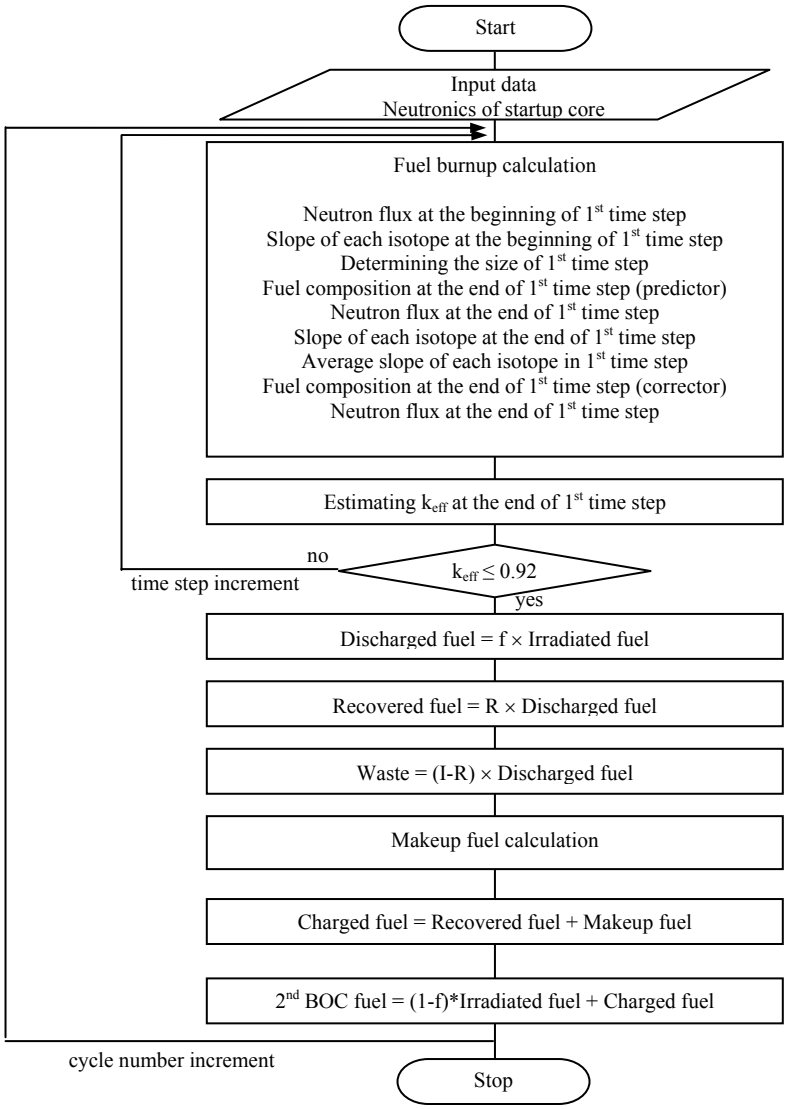

Figure 2.4 Flow chart for code programming

4 Computation for Single Cycle Case

4.1 Reference LBE-Cooled Transmuter

A computer code, WACOM, has been developed to implement the model described in Chapters 2 & 3. For simulation of an ATW system, the neutronics (ϕ, σ, $\cdots$) of the ATW transmuter need to be known because WACOM uses those as part of input data. In this chapter, the LBE-cooled transmuter point design [12] proposed by Los Alamos National Laboratory (LANL) is utilized for the ATW fuel cycle simulation.

The blanket of the proposed LBE-cooled transmuter is shown in Figure 4.1. It consists of 19 hexagonal lattice positions containing the lead-bismuth eutectic (LBE) target/buffer and 192 fuel assemblies. The blanket is surrounded by two hexagonal rows of reflector assemblies and one row of B_4C shield assemblies. The principal design parameters of the proposed design are summarized in Table 4.1. A semi-annual 6-batch fuel management scheme is employed with the capacity factor of 75%.

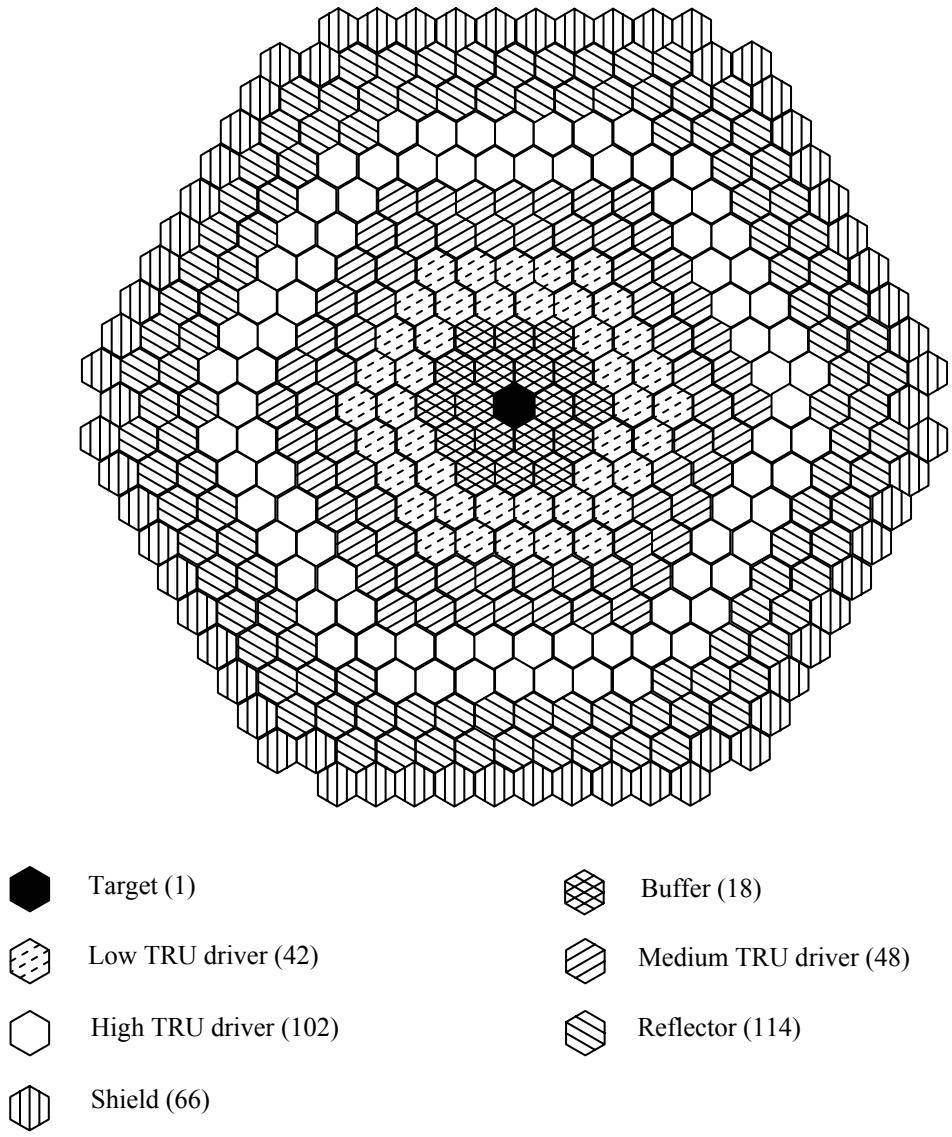

Figure 4.1 Proposed LBE-Cooled blanket configuration (192 fuel assemblies)

Table 4.1 Design Parameters for the Proposed LBE-Cooled Blanket Point Design [ ]

Proton Energy (GeV)	1
Target Material	LBE
Fuel Material	(TRU-10Zr)-Zr
Pin Diameter (cm)	0.635
Cladding Thickness (cm)	0.056
Pitch-to-Diameter Ratio	1.727
Number of Pins per Assembly	217
Fuel Smear Density (%)	75

Volume Fraction (at operating temperature)	Fuel	0.140
	Structure	0.103
	Coolant	0.695
Hexagonal Assembly Pitch (cm)		16.142
Number of Assemblies	LBE target/buffer	19
	Fuel	192
	LBE Reflector	114
	Shield	66
TRU Fraction Split Factor (outer/middle/inner zone)		1.45/1.28/1.00
Active Fuel Height (cm)		106.68
Equivalent Fuel Region Diameter (cm)		246.21
Maximum Blanket Diameter (cm)		357.07
Number of Fuel Batches	Inner zone	5
	Middle and Outer Zones	6

4.2 Neutronics of Start-up Core of the LBE-Cooled Transmuter

Figure 4.2 shows the simplified LBE-cooled point design geometry used for the MCNP simulation. It is assumed that the reactor has a cylindrical geometry with three regions: the target region, the fuel region, and the reflector region. The inner region is a spallation target with a radius of 36.9 cm, the middle region is the homogenized fuel region with a radius of 123.1 cm, and the outer region is the reflector region with a radius of 152.8 cm. The shield is not considered for simplicity. The active fuel height is 106.7 cm and the height of the reactor is assumed to be 500 cm. The homogenized fuel region is composed of fuel, coolant, and structure material and their volume fractions are assumed to be 14.9%, 74.1%, and 11.0% instead of 14.0%, 69.5%, and 10.3% respectively of Table 4.1 to make the total homogenized volume fraction be unity.

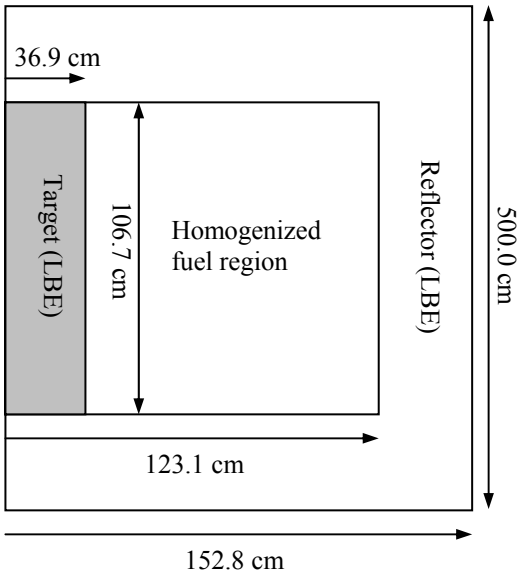

Figure 4.2 Simplified LBE-Cooled point design geometry used for the MCNP simulation

The properties and composition of the TRU taken from PWR-spent fuel and the properties of Zr in the homogenized fuel region are given in Table 4.2.

Table 4.2 Fuel Isotope Properties and PWR-TRU Composition [8][12][13]

i	Isotope	Atomic mass [amu]	Nominal density [g/cm^3]	Isotopic density [g/cm^3]	$t_{1/2}$ [s]	Average fission energy [MeV]	MPC for ingestion [Ci/*l*]	Weight fraction in TRU[a]
1	U234	234.041	18.95	18.631	7.7160E+12	201.7	3E-10	0.0000
2	U235	235.044		18.811	2.2201E+16	201.7	3E-10	4.0000E-05
3	U236	236.046		18.891	7.3794E+14	201.7	3E-10	2.0000E-05
4	U238	238.051		19.052	1.4097E+17	201.7	3E-10	4.7800E-03
5	Np237	237.048	20.25	20.450	6.7487E+13	206.1	2E-11	5.0230E-02
6	Pu238	238.050	19.84	19.332	2.7121E+09	210.2	2E-11	1.2720E-02
7	Pu239	239.052		19.413	7.6948E+11	210.6	2E-11	5.3196E-01
8	Pu240	240.054		19.494	2.0751E+11	211.0	2E-11	2.1534E-01
9	Pu241	241.057		19.576	4.1628E+08	211.3	1E-09	3.7820E-02
10	Pu242	242.059		19.657	1.1952E+13	211.7	2E-11	4.6850E-02

11	Am241	241.057	13.67	13.557	1.3630E+10	215.2	2E-11	8.9670E-02
12	Am242m	242.060		13.614	4.4466E+09	215.5	2E-11	1.4000E-04
13	Am243	243.061		13.670	2.3242E+11	215.9	2E-11	9.2600E-03
14	Cm242	242.059	13.67	13.236	1.4083E+07	219.4	7E-10	0.0000
15	Cm243	243.061		13.291	9.4608E+08	219.8	3E-11	2.0000E-05
16	Cm244	244.063		13.346	5.7080E+08	220.2	3E-11	1.0400E-03
17	Cm245	245.066		13.400	2.6806E+11	220.5	2E-11	9.0000E-05
18	Cm246	246.067		13.455	1.5011E+11	220.9	2E-11	1.0000E-05
	Zr	91.22	6.49	6.49	—			

[a] Corresponding to a 25 year cooled PWR-TRU assuming that 99.995% of the uranium is removed in the UREX process

The proposed LBE-cooled reactor has a lead-bismuth eutectic (LBE) as its coolant. The composition and properties of LBE-coolant are shown in Table 4.3. The density of the LBE-coolant is assumed 10.151 g/cm^3 at the temperature of 475 ^{o}C.

Table 4.3 Composition and Properties of LBE-Coolant [14][15]

Isotope	Nominal density [g/cm^3]	Weight fraction in coolant
Pb	11.34	4.45E-01
Bi-209	9.80	5.55E-01

Table 4.4 shows the properties of HT-9, the structural material assumed for the reactor. The density of HT-9 is assumed to be 7.66 g/cm^3 at 475 ^{o}C.

Table 4.4 Composition and Properties of Structure Material HT-9 [16]

Element	Nominal density [g/cm^3]	Weight fraction in structure
Fe	7.87	8.5E-01
Cr	7.19	1.15E-01
Ni	8.90	5.0E-03
Mo	10.20	1.0E-02
Mn	7.43	6.0E-03
C	1.60	2.0E-03

Si	2.33	4.0E-03
W	19.20	5.0E-03
V	6.10	3.0E-03

The fuel composition at the beginning of the each cycle is determined such that the beginning of cycle (BOC) k_{eff} of the homogenized reactor core is 0.98. The cycle proceeds until k_{eff} drops to 0.92. The value of the fuel composition at BOC is controlled by adjusting the ratio of actinides to zirconium. It is found that the first BOC fuel composition satisfying the k_{eff} constraint has 31.8 wt% actinide and 68.2 wt% zirconium. The effective one group cross sections for three types of neutron reactions, (n,γ), (n,f), and (n,2n) as calculated by MCNP for the start-up core are listed in Table 4.5.

Table 4.5 Effective One Group Cross Sections of the Start-up Core (Actinide-31.8 wt%, Zr-68.2 wt%)

Isotope	(n,γ) [b]	(n,2n) [b]	(n,f) [b]
U234	6.926E-01	5.980E-05	3.362E-01
U235	5.428E-01	4.337E-04	1.928E+00
U236	4.723E-01	3.065E-04	8.383E-02
U238	3.709E-01	5.409E-04	2.748E-02
Np237	1.597E+00	1.213E-04	3.189E-01
Pu238	7.624E-01	1.706E-04	1.145E+00
Pu239	5.213E-01	2.309E-04	1.827E+00
Pu240	5.314E-01	9.162E-05	3.726E-01
Pu241	4.565E-01	7.841E-04	2.566E+00
Pu242	4.741E-01	2.408E-04	2.570E-01
Am241	1.731E+00	2.627E-05	2.451E-01
Am242m	4.254E-01	4.409E-04	4.166E+00
Am243	1.536E+00	2.981E-05	1.906E-01
Cm242	3.558E-01	6.844E-06	1.279E-01
Cm243	2.718E-01	4.210E-04	2.834E+00
Cm244	8.806E-01	1.434E-04	4.223E-01
Cm245	3.183E-01	7.587E-04	2.508E+00
Cm246	2.509E-01	1.916E-04	2.454E-01

4.3 Fuel Inventory Evolution in the Reference LBE-Transmuter for a Single Cycle

Using the cross section data listed in Table 4.5, fuel inventory evolution in the reference LBE-cooled transmuter for the start-up cycle was calculated. Assumptions used for this calculation include the following: (1) The reactor power is 840 MWt. (2) The irradiation time is determined by the constraint $0.92 \leq k_{eff} \leq 0.98$. (3) The cross section values used are constant during the irradiation. (4) The mass of zirconium contained in fuel is not affected by neutron irradiation. It is observed that the mass fraction of actinides in the core decreases from ~31.8% at the beginning of the start-up cycle to ~29.6% at the end of the start-up cycle. This could be interpreted that ~6.9 % actinide was transmuted into fission products during the irradiation period. The irradiation period that takes for the value of k_{eff} to reaches to 0.92 was ~108 days for the start-up cycle. Fractional mass changes of actinide, fission product, and zirconium for the start-up cycle is shown in Table 4.6 and the isotopic composition change of actinide for the start-up cycle in Table 4.7 in the unit of number of atoms. In the last column of Table 4.7, positive or negative sign represents an increase or a decrease in the amount of an isotope during the cycle, respectively. Several isotopes such as ^{235}U, ^{238}U, ^{237}Np, ^{239}P, ^{241}Pu, and ^{241}Am show reduction in their amount while other isotopes increasing by neutron irradiations.

Table 4.6 Fractional Mass Changes of Actinide, Fission Product, and Zirconium for the Start-up Cycle

	Actinides	Fission Products	Zirconium
BOC (t=0)	31.8%	0	68.2%
EOC (t=108days)	29.6%	2.2%	68.2%

Table 4.7 Isotopic Composition Change of Actinide for the Start-up Cycle

Isotope	BOC (t=0)	EOC (t=108days)	Fractional change
U234[a]	1.0000E+1	1.1238E+23	+1.124E+23
U235	1.3776E+23	1.3445E+23	-2.403E-02
U236	6.8586E+22	9.3094E+22	+3.573E-01
U238	1.6254E+25	1.5875E+25	-2.332E-02
Np237	1.7152E+26	1.5327E+26	-1.064E-01
Pu238	4.3253E+25	5.6684E+25	+3.105E-01
Pu239	1.8013E+27	1.5699E+27	-1.285E-01
Pu240	7.2614E+26	7.3885E+26	+1.750E-02
Pu241	1.2700E+26	1.2553E+26	-1.157E-02
Pu242	1.5670E+26	1.5735E+26	+4.148E-03
Am241	3.0111E+26	2.6959E+26	-1.047E-01
Am242m	4.6818E+23	5.4560E+24	+1.065E+01
Am243	3.0839E+25	3.2107E+25	+4.112E-02
Cm242[a]	1.0000E+1	1.5294E+25	+1.529E+25
Cm243	6.6607E+22	2.2101E+23	+2.318E+00
Cm244	3.4493E+24	5.8992E+24	+7.103E-01
Cm245	2.9728E+23	4.7786E+23	+6.074E-01
Cm246	3.2896E+22	3.8996E+22	+1.854E-01

[a] The number of atoms at the beginning of irradiation was assumed as 1E+00

4.4 Benchmarking of WACOM against MOCUP for a Single Cycle

To check the isotope depletion module of the developed model, it was compared to the depletion module of MOCUP [4] utility, a code package that couples MCNP [7] for particle transport calculations and ORIGEN 2 [6] for isotope depletion calculations. The proposed LBE-cooled transmuter point design described in Section 4.1 has been used for benchmarking. Before comparing, the characteristics of MOCUP are briefly reviewed and differences between MOCUP and WACOM will be discussed.

MOCUP is a series of utility and data manipulation programs to solve time- and space-dependent coupled neutronics/isotopics problems. The neutronics calculation is performed by the Los Alamos National Laboratory code system, MCNP version 4a or later (CCC-200

or CCC-660), and the depletion and isotopics calculation are performed by CCC-371/ORIGEN2.1 developed at Oak Ridge National Laboratory. MOCUP consists of three utility programs (mcnpPRO, origenPRO, compPRO) to, respectively, search the MCNP output and tally files for relevant cell and tally parameters, prepare ORIGEN2.1 input files and execute the ORIGEN2.1 runs and search ORIGEN2.1 punch files for relevant isotope concentrations and produce new MCNP input files.

MCNP Post-processor (mcnpPRO) provides the cell fluxes and the radiative capture, alpha production, fission, (n,2n), and (n,3n) cross sections for the ORIGEN2.1 calculation through the MOCUP intermediate file, which is referred to as the MCNP processor output file. The MCNP fluxes are adjusted by the flux multiplier table. The ORIGEN2.1 Pre-processor (origenPRO) takes the flux and cross section information from the MCNP processor output files and merges it into the skeletal ORIGEN2.1 input files to create modified ORIGEN2.1 input files for each MCNP cell to be depleted. ORIGEN2.1 Pre-processor (origenPRO) can also execute ORIGEN2.1 for each input file and prepare the newly generated composition data for the next time sequence.

While the reaction types which MCNP Post-processor recognizes are limited to (n,γ) reaction, (n,2n) reaction, (n,3n) reaction, fission reaction, and alpha production, the skeletal file for ORIGEN2.1 requires a complete cross section/yield specification for each time-dependent isotope. (n,γ^*) and (n,2n*) cross section data which are required for ORIGEN2.1 is not provided by MCNP and thus those are copied from the ORIGEN2.1 cross section library.

However, WACOM, the model developed here, is supposed to use MCNP-generated cross section data and does not have any cross section library like ORIGEN2.1 cross section libraries. Therefore, in order to compare this model with MOCUP using the similar input data, (n,γ^*) and $(n,2n^*)$ cross section data of ORIGEN2.1 cross section library are manually added to the effective one group (n,γ) and (n,2n) cross sections generated by MCNP, respectively. The branching ratio of (n,γ) and (n,γ^*) cross section and that of (n,2n) and $(n,2n^*)$ are used to simulate the neutron-induced reaction of an isotope which has both ground state cross section and excitation cross section. For example, letting δ as the ratio of (n,γ) cross section to the combined cross section of (n,γ) and (n,γ^*) cross section, $(1-\delta)$ represents the ratio of (n,γ^*) cross section to the combined cross section of (n,γ) and (n,γ^*) cross section. In ORIGEN2.1, ^{241}Am and ^{243}Am have both (n,γ) and (n,γ^*) cross section. ^{241}Am leads to ^{242}Am and ^{242m}Am by (n,γ) and (n,γ^*) reactions, respectively. ^{243}Am leads to ^{244}Am and ^{244m}Am by (n,γ) and (n,γ^*) reaction, respectively.

The effective one group cross-sections of the LBE-cooled ATW reactor have been calculated with MCNP for its start-up core that has a 31.8 weight % of HM and a 68.2 weight % of Zr. Table 4.5 shows the obtained effective one-group cross sections. For the fission product (FP), a pseudo cross section has been estimated under the assumption that the estimated neutron absorption rate by fission products in MOCUP is equal to the neutron absorption rate by fission products calculated from this model.

To estimate the effective cross sections of isotopes in homogenized fuel, target, and reflector regions, several cross section data sources such as ENDF/B-IV and ENDF/B-V were used by MCNP. The operating temperatures of the proposed LBE-cooled reactor are

assumed to be ~1000 ^{o}K in fuel and target, ~750 ^{o}K in structure and ~700 ^{o}K in reflector. Due to the unavailability of cross section data sources at operating temperature levels, the effective cross sections of some isotopes such as Np-isotopes, Am-isotopes, Cm-isotopes, HT-9 constituents, and LBE constituents were estimated at the room temperature rather than their operating temperatures. Thus, the estimated effective cross sections of those materials could be deviated to some extent from those expected at their operating temperatures.

In addition to the unavailability of excitation cross section and insufficient cross section libraries at reactor operating temperatures in MCNP, the cross section data source of ^{242}Am which is approximated in Figure 2.2 is not found in MCNP cross section libraries. However, ORIGEN2.1 has the cross section data of it in its own cross section library and uses them. From the facts described so far, it is obvious that MOCUP uses two different kinds of cross section data, one is provided by MCNP and the other comes from the cross section library of ORIGEN2.1 to calculate isotope depletion and generation. Except for benchmarking purpose, WACOM uses MCNP-generated cross section and does not consider excitation cross sections. This could make significant difference in the concentrations of americium and curium isotopes when comparing to the MOCUP calculation or other tools taking into account excitation reactions in their isotope depletion module. The cross section data sets in Table 4.5 were used for the benchmarking against MOCUP but the capture cross sections of ^{241}Am and ^{243}Am have been modified such that they include both ground state cross section and excitation cross section. The modified capture cross section of ^{241}Am is 1.7279 [b] and that of ^{243}Am is 2.1780 [b].

Table 4.8 compares the fractional changes of the fuel isotopes in the reactor after an irradiation time of 1year for a single cycle. The fractional change is obtained by dividing the number of atoms of each isotope at the end of irradiation by its number of atoms at the beginning of irradiation. A very good agreement is found between WACOM and MOCUP.

Table 4.8 Fractional Changes of Fuel Isotopes for Irradiation time of 1 year

Isotopes	MOCUP	WACOM	Relative difference
U234[a]	2.4779E+23	2.4782E+23	0.01%
U235	1.1303E+00	1.1304E+00	0.01%
U236	2.1522E+00	2.1447E+00	0.35%
U238	9.5655E-01	9.5647E-01	0.01%
Np237	7.9779E-01	7.9777E-01	0.00%
Pu238	1.7643E+00	1.7699E+00	0.32%
Pu239	7.4899E-01	7.4900E-01	0.00%
Pu240	1.0006E+00	1.0005E+00	0.01%
Pu241	9.3182E-01	9.2832E-01	0.38%
Pu242	1.0033E+00	1.0033E+00	0.00%
Am241	7.7279E-01	7.7430E-01	0.20%
Am242m	2.0488E+01	2.0501E+01	0.06%
Am243	9.5276E-01	9.5288E-01	0.01%
Cm242[a]	3.3372E+25	3.3481E+25	0.33%
Cm243	6.9254E+00	6.9373E+00	0.17%
Cm244	3.1975E+00	3.1994E+00	0.06%
Cm245	2.8720E+00	2.8717E+00	0.01%
Cm246	1.5125E+00	1.5120E+00	0.03%

[a] The number of atoms at the beginning of irradiation was assumed as 1E+00

4.5 Discussions and Conclusions

The simplified model and computer code developed for efficient simulation of the evolution of the fuel and waste composition and inventory in ATW systems, taking into account constraints on the reactor core design, are functional. The information that can be provided by the newly developed tool is useful for parametric studies of the impact of different transmutation systems design on the waste and repository assessment. Before

applying the newly developed tool to actual analysis of transmutation systems it is necessary to work out an algorithm that will adjust the effective one group cross section and leakage probability to the variation in the actinide loading and composition.

For the LBE-cooled transmuting reactor considered in this work the variation in the effective one group and leakage probability between the first cycle and the equilibrium cycle is found to be within 20%. An algorithm will be developed for the WACOM code to linearly interpolate the cross sections and leakage probability between two data vectors to be generated with MCNP for the first cycle and nearly equilibrium cycle.

5 Multi Cycle Calculation

5.1 Introduction

A mathematical model and computer code, WACOM, for the analysis of an ATW fuel cycle has been developed and its applicability to a reference transmuter design has been investigated in the previous chapter. The results show that for reliable prediction of the ATW fuel cycle evolution WACOM needs to account for the variation of the effective one group cross sections with the change in the inventory and composition of the fuel loaded into the ATW. The purpose of this chapter is to develop a computational scheme for accomplishing this. The conventional approach in fuel cycle analysis is to re-calculate the reactor spectrum and effective one group cross sections at least once and often several times in one cycle, i.e., between refuelings. For multi-cycle analyses this approach requires significant effort and computational time, especially when using a Monte-Carlo based code, such as MCNP, for the neutronic calculations.

An alternative approach involving use of interpolation of pre-prepared effective one group cross sections is investigated in this work. Using the interpolation method developed, the effect of difference in reported values of the branching ratio of ^{241}Am on the results of multi-cycle analyses is also investigated.

5.2 Methodology

5.2.1 Neutron Spectrum Variation

In order to check if the fuel composition variation predicted by WACOM satisfies the k_{eff} constraint well enough, the k_{eff} values of several BOC and EOC fuel compositions have been estimated by MCNP. Significant discrepancies were found between the k_{eff} constraint and estimated k_{eff} values. For example, the k_{eff} value of the 100^{th} BOC fuel is estimated to be 1.022 by MCNP, which should be around 0.98. This implies that variation of neutron spectrum with the fuel composition needs to be taken into account.

The effect of neutron spectrum variation in the reactor core is investigated by considering the BOC fuel composition of several of the cycles plotted in Figure 5.1. Table 5.1 shows the effective one group (n,γ) cross sections for the selected cycles as estimated by MCNP. The variation pattern of the (n,γ) cross sections of the U isotopes are plotted in Figure 5.2 with respect to the mass fraction of actinide in the fuel. It is noticed that the (n,γ) cross sections of the U isotopes vary almost linearly with the mass fraction of the actinides in the fuel. A similar behavior is observed for the other isotopes and also for the (n,f) cross sections. It is concluded that it is sufficient to calculate with MCNP one set of effective one group cross sections for two different fuel loadings. The effective one group cross sections for any composition can then be estimated by interpolation and extrapolation. The two fuel compositions chosen as the basis for the interpolation are the composition at the beginning of the first cycle and the composition at the equilibrium cycle that is calculated in Figure 5.1. The results from these two MCNP calculations are used for developing two linear fits for each isotope; one for (n,γ) and the other for (n,f) cross sections, with respect to the mass

fraction change of actinide in the fuel. The (n,2n) cross sections are assumed to be constant through all cycles due to their small contribution to the isotopic transmutation.

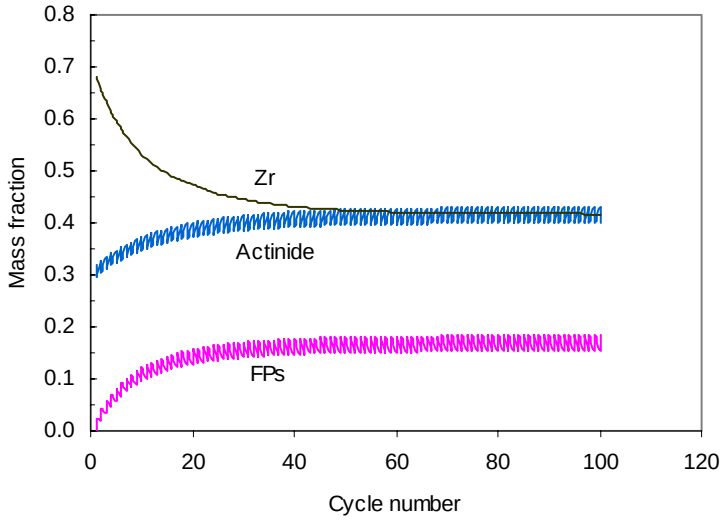

Figure 5.1 Fuel composition change with cycle number predicted by using the effective one group cross sections of the start-up core

Table 5.1 Effective One Group (n,γ) Cross Sections of Several Fuel Compositions Estimated by MCNP

isotope	1st cycle (31.8%Ac)	10th cycle (37.2%Ac)	20th cycle (40.0%Ac)	100th cycle (43.0%Ac)
U234	6.926E-1	5.748E-1	5.550E-1	5.240E-1
U235	5.428E-1	4.867E-1	4.767E-1	4.520E-1
U236	4.723E-1	4.026E-1	3.930E-1	3.730E-1
U238	3.709E-1	3.137E-1	3.056E-1	2.870E-1
Np237	1.597E+0	1.423E+0	1.390E+0	1.320E+0
Pu238	7.624E-1	6.780E-1	6.641E-1	6.300E-1
Pu239	5.213E-1	4.459E-1	4.313E-1	3.990E-1
Pu240	5.314E-1	4.609E-1	4.478E-1	4.230E-1
Pu241	4.565E-1	4.051E-1	3.948E-1	3.740E-1
Pu242	4.741E-1	4.114E-1	3.987E-1	3.740E-1
Am241	1.731E+0	1.540E+0	1.508E+0	1.430E+0
Am242m	4.254E-1	3.561E-1	3.427E-1	3.140E-1
Am243	1.536E+0	1.341E+0	1.308E+0	1.230E+0
Cm242	3.558E-1	2.941E-1	2.806E-1	2.560E-1
Cm243	2.718E-1	2.278E-1	2.198E-1	2.020E-1

Cm244	8.806E-1	7.824E-1	7.660E-1	7.240E-1
Cm245	3.183E-1	2.887E-1	2.838E-1	2.710E-1
Cm246	2.509E-1	2.159E-1	2.074E-1	1.950E-1
Zr	2.887E-2	2.232E-2	2.206E-2	2.133E-2
FP	2.662E-1	2.604E-1	2.523E-1	2.364E-1

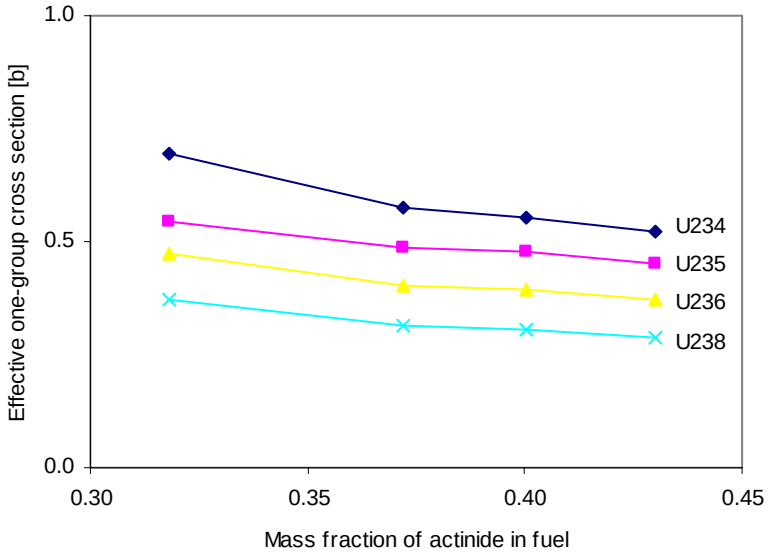

Figure 5.2 Variations of effective one-group (n,γ) cross sections of U-isotopes with respect to the mass fraction of actinide in fuel

5.2.2 Validation of Interpolating Scheme for Estimation of Neutronics

Figure 5.3 shows the fuel composition variation with cycle number predicted by WACOM with an interpolating scheme to account for neutronic variations. This figure shows profiles similar to those in Figure 5.1 but it has a smaller concentration of actinide and a larger concentration of zirconium at the equilibrium cycles. The mass fraction of actinides increases from ~32% at start-up to ~41% rather than ~43% at the beginning of the equilibrium cycle. To check whether the fuel compositions predicted by WACOM (Figure 5.3) satisfy the k_{eff} constraint, several fuel compositions at beginning of cycle and end of

cycle are chosen arbitrarily and their k_{eff} and effective one group cross section values are calculated by MCNP. Table 5.2 shows that the k_{eff} values calculated by MCNP are within ~0.5% of the k_{eff} constraints. This confirms that the profile plotted in Figure 5.3 represents adequately the cycle dependent fuel composition variation of the ATW system. Table 5.3 compares the interpolated cross sections at the beginning of the 100th cycle with the effective one group cross sections calculated by MCNP for the WACOM calculated composition. The interpolated cross sections are in good agreement with those estimated by MCNP. This indicates that the interpolation scheme used to update the effective one group cross sections is satisfactory and can be used for the ATW fuel cycle analyses.

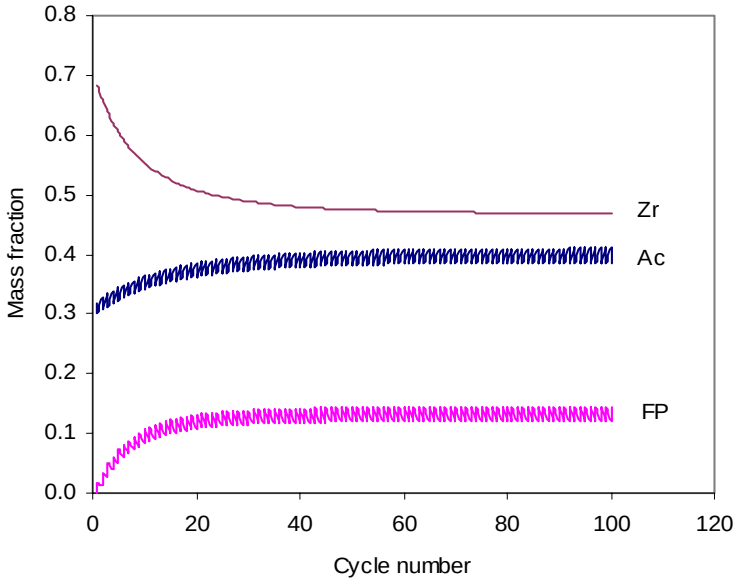

Figure 5.3 Fuel composition variation with cycle number predicted by using interpolated neutronics

Table 5.2 k_{eff} -Values of 10^{th}, 20^{th}, and 100^{th} Fuel Composition in Figure 3.5 Estimated by MCNP

Cycle	10^{th} cycle	20^{th} cycle	100^{th} cycle
BOC[a]-k_{eff}	0.984 (±0.001)	0.982 (±0.001)	0.979 (±0.001)
EOC[b]-k_{eff}	0.925 (±0.001)	0.925 (±0.001)	0.922 (±0.001)

[a] beginning of cycle, [b] end of cycle

Table 5.3 Comparison of Interpolated Capture Cross Sections with MCNP-Estimated Capture Cross Sections for the BOC Fuel Composition at the 100^{th} cycle

isotope	MCNP [b]	Interpolated [b]	Relative difference
U234	5.546E-01	5.536E-01	0.18%
U235	4.735E-01	4.680E-01	1.16%
U236	3.922E-01	3.904E-01	0.46%
U238	3.020E-01	3.017E-01	0.10%
Np237	1.382E+00	1.369E+00	0.94%
Pu238	6.592E-01	6.533E-01	0.90%
Pu239	4.275E-01	4.204E-01	1.66%
Pu240	4.444E-01	4.421E-01	0.52%
Pu241	3.916E-01	3.885E-01	0.79%
Pu242	3.917E-01	3.916E-01	0.03%
Am241	1.498E+00	1.483E+00	1.00%
Am242m	3.390E-01	3.336E-01	1.59%
Am243	1.301E+00	1.284E+00	1.31%
Cm242	2.765E-01	2.736E-01	1.05%
Cm243	2.175E-01	2.143E-01	1.47%
Cm244	7.578E-01	7.515E-01	0.83%
Cm245	2.821E-01	2.793E-01	0.99%
Cm246	2.073E-01	2.048E-01	1.21%

5.2.3 Revised Flow Chart of WACOM Code

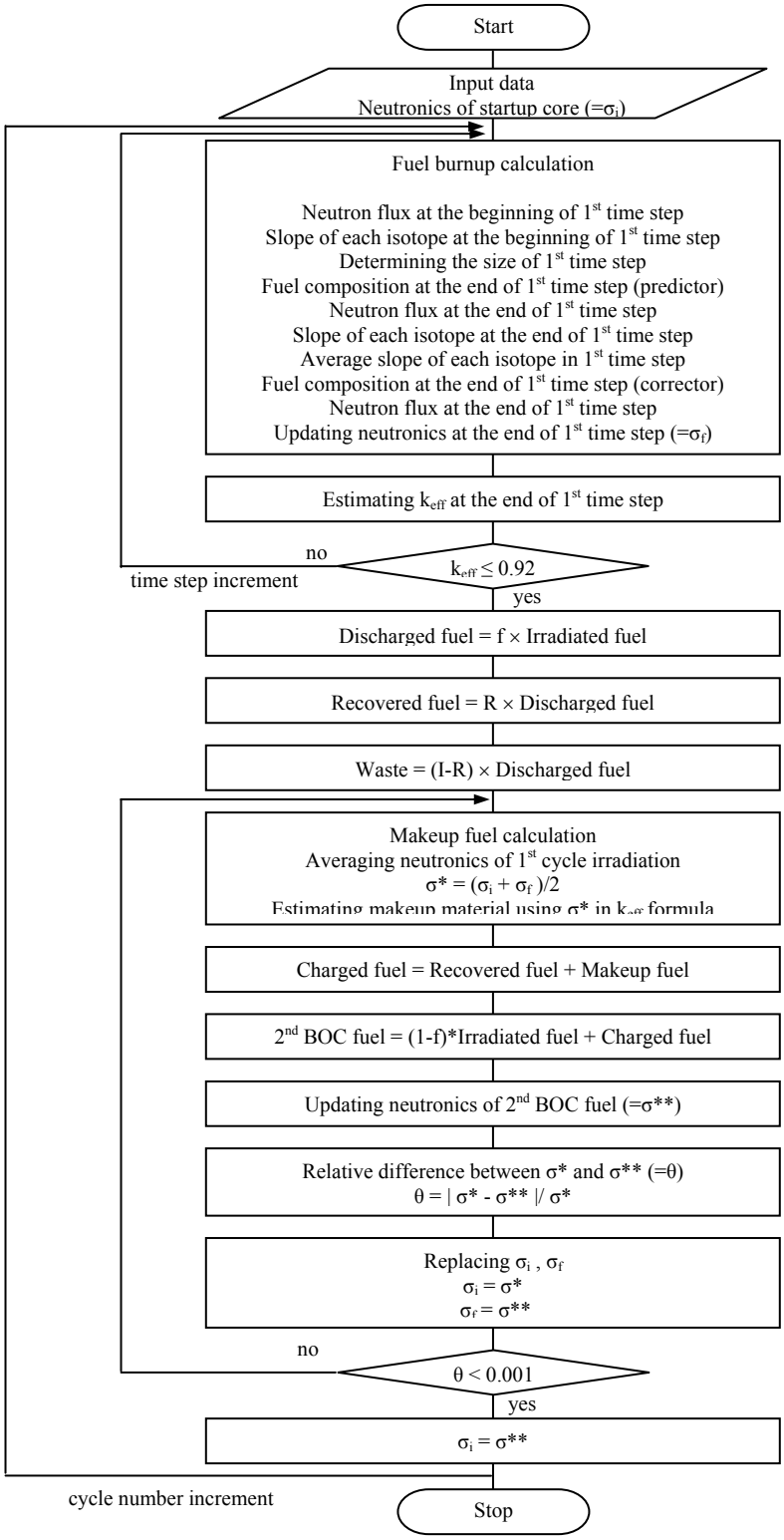

Figure 5.4 Revised flow chart of WACOM code

5.3 Analysis of the Reference LBE-Cooled Transmuter

The performance of the reference LBE-cooled transmuter was assessed by modified WACOM described in section 5.2. Used input data are listed in Table 4.2 and 4.5 and following operating conditions are assumed: (1) the cycle duration is controlled by bounding the range of k_{eff} variation from 0.98 to 0.92, (2) the recovery fraction of each TRU element by partitioning is 0.999 and recovered TRU is free from fission products, (3) the fuel discharge fraction is 1/6 although the burnup is assumed to be uniform across the blanket, (4) the reactor power is 840 MWt, (5) no cooling time for discharged fuel is assumed, (6) TRU composition of feed material is constant at that of SNF from PWR after 25-year cooling and 99.995% uranium removal, (7) no mass loss from fuel fabrication process is assumed, and (8) except fuel irradiation in reactor core, all processes are performed instantaneously. For (8), current version of WACOM model does not take into account the cooling time of discharged fuel before and during separation process, the cooling time of accumulating TRU waste from the separation process, and the time required for refueling in each cycle.

The evolution of the core inventory in the reference transmuter is given in Figure 5.3. Figure 5.5 shows the corresponding evolution of the cycle duration. It is estimated that cycle duration of LBE-cooled transmuter will increase from ~86 days for the start-up cycle to ~144 days for the equilibrium cycle while the actinides mass fraction increases from ~32% to ~41%. It takes nearly 60 cycles to approach the equilibrium cycle, with most of the variations taking place during the first 20 cycles or so.

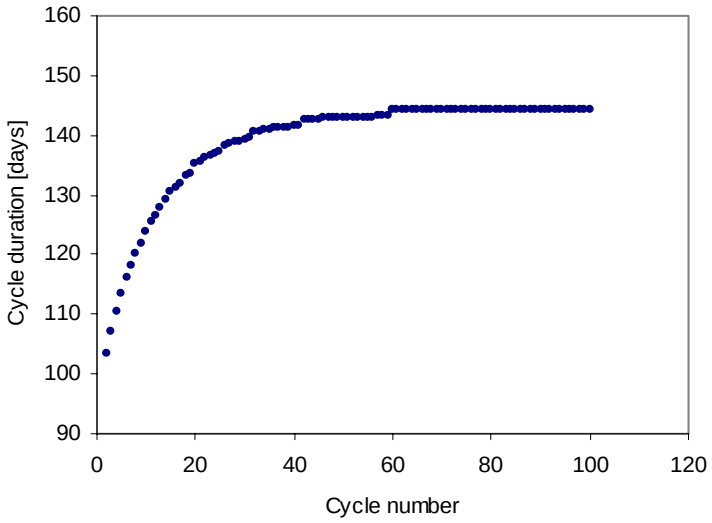

Figure 5.5 Cycle duration of the LBE-cooled ATW system

Figure 5.6 shows the cycle dependent in-core inventory of fuel isotopes in the reactor. Most nuclides exhibit a zigzag pattern which is due to the transmutation followed by fuel makeup. The difference between the top and the bottom points in the zigzag represents the amount of a nuclide transmuted in the given cycle. ^{237}Np, ^{239}Pu, and ^{241}Am have relatively high fractional transmutation per cycle. The concentration of most of nuclide except zirconium increases with cycle number until it reaches a steady state although some Cm isotopes such as ^{244}Cm, ^{245}Cm, and ^{246}Cm do not reach a steady-state even in 100 cycles. The increase in the mass fraction of actinides in the fuel compensates the reactivity loss due to fission products buildup and the change in the actinide composition. For example, the atomic fraction of ^{239}Pu that has a large fission-to-capture cross section ratio decreases from ~53% to ~24% while that of ^{240}Pu that has a small fission-to-capture cross section increases from ~22% to ~35%. Table 5.4 shows the isotopic composition of actinide in the start-up core and in the equilibrium core. The capture-to-fission ratios of actinides in the start-up

core and in the equilibrium core are listed in Table 5.5. All actinides show decreased capture-to-fission ratios in the equilibrium core compared to the start-up core.

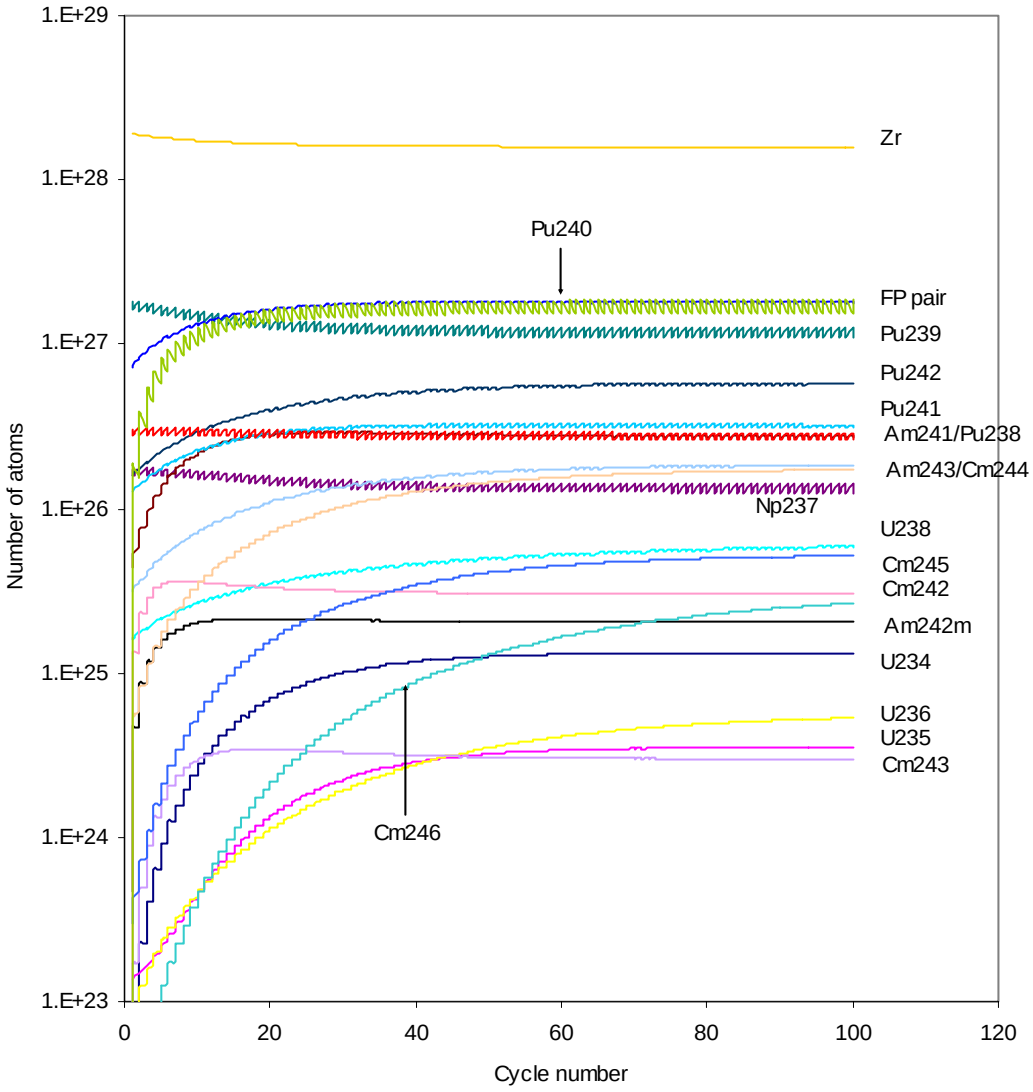

Figure 5.6 Cycle dependent in-core inventory of fuel isotopes in the LBE-cooled ATW system

Table 5.4 Isotopic Composition of Actinide in the Start-up Core and the Equilibrium Core

Isotope	Start-up (at %)	Equilibrium (at %)
U234	0.000%	0.251%
U235	0.004%	0.067%
U236	0.002%	0.101%
U238	0.481%	1.124%
Np237	5.077%	2.674%
Pu238	1.280%	5.240%
Pu239	53.314%	23.936%
Pu240	21.492%	34.581%
Pu241	3.759%	6.164%
Pu242	4.638%	11.093%
Am241	8.912%	5.490%
Am242m	0.014%	0.386%
Am243	0.913%	3.509%
Cm242	0.000%	0.572%
Cm243	0.002%	0.057%
Cm244	0.102%	3.270%
Cm245	0.009%	0.980%
Cm246	0.001%	0.503%

Table 5.5 Capture to Fission Ratios of Actinides in the Start-up Core and the Equilibrium Core

Isotope	Start-up	Equilibrium
U234	2.06	1.61
U235	0.28	0.27
U236	5.63	4.56
U238	13.50	10.43
Np237	5.01	4.21
Pu238	0.67	0.59
Pu239	0.29	0.25
Pu240	1.43	1.17
Pu241	0.18	0.17
Pu242	1.84	1.48
Am241	7.06	5.93
Am242m	0.10	0.09
Am243	8.06	6.61
Cm242	2.78	2.07
Cm243	0.10	0.09
Cm244	2.09	1.76
Cm245	0.13	0.13
Cm246	1.02	0.82

Figure 5.7 shows fractional transmutation of actinide with cycle number. *Fractional transmutation of actinide is defined as the ratio of the difference between the amount of an isotope in the fuel at BOC and that at EOC to that at BOC within a cycle*. Each actinide in reactor core experiences increase or decrease in its concentration during irradiation. In Figure 5.7, positive value means that the amount of an isotope decreases during the cycle and negative value implies that it increases during the cycle. As observed in figure, we can see that ^{237}Np, ^{239}Pu, and ^{241}Am have relatively large positive fractional transmutations(more than ~10%), whereas other Pu isotopes, ^{238}U, and ^{243}Am have very small positive fractional transmutations (less than ~3%). Most of U and Cm isotopes show buildup in the reactor at early cycles even though they eventually approach to zero, which means no depletion or accumulation of those nuclides in the fuel by recycling.

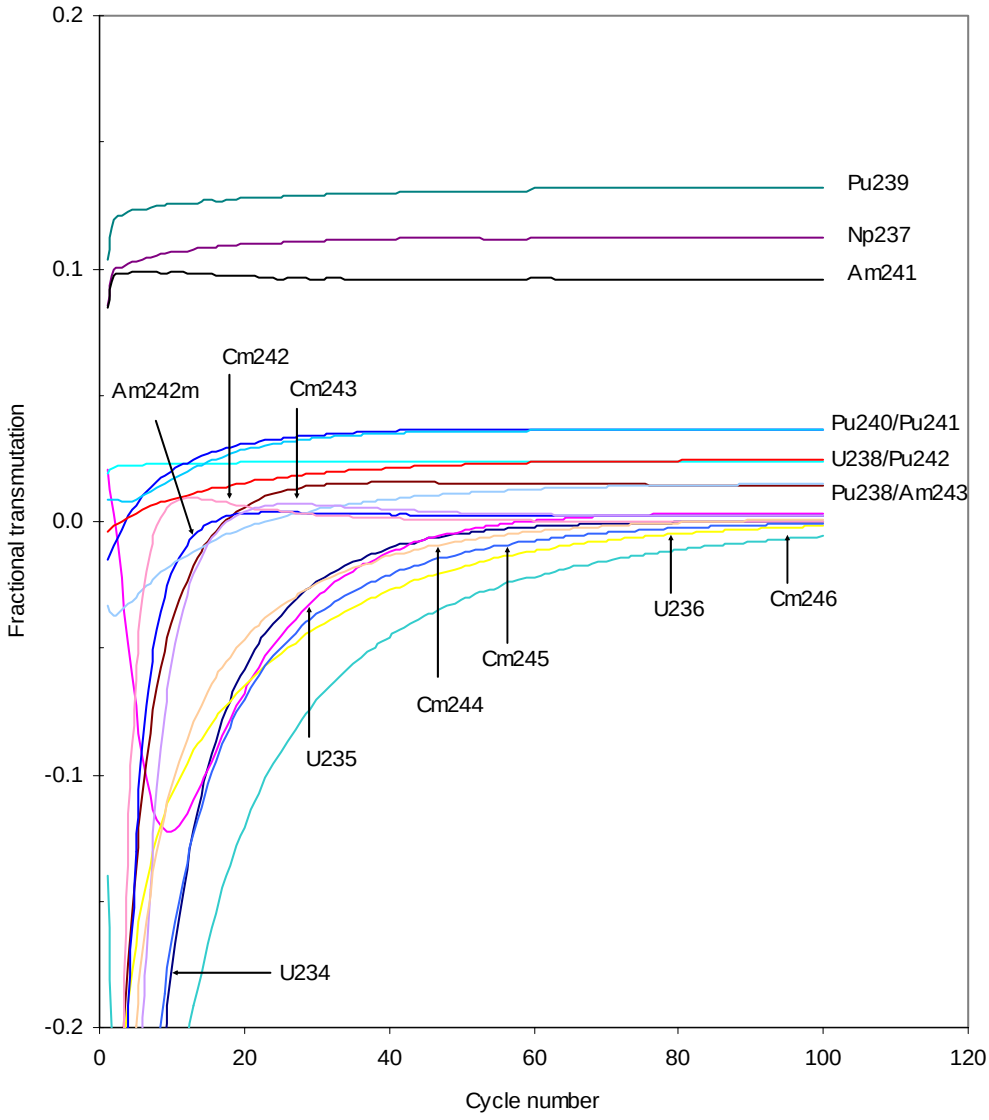

Figure 5.7 Fractional transmutation of actinide with cycle number

Figure 5.8 shows the cumulative mass reduction ratio of actinide with the cycle number for two cases. *The cumulative waste reduction ratio is defined as the cumulative amount of an isotope up to the n-th cycle in the waste stream divided by the cumulative amount of the same isotope up to the n-th cycle fed to the ATW system in the makeup stream*. The ratio means to what extent actinide inventory can be reduced by the ATW system after a certain

number of cycles. A small reduction ratio is desirable. Figure 5.8 represents the case that the actinide in the start-up core and in the core to be decommissioned is not considered as makeup or waste. The cumulative inventory of actinide in both waste and makeup stream increases almost linearly but the difference between two inventories in waste and makeup becomes reduced little by little as the cycle number increases. Therefore, the cumulative mass reduction ratio increases with the cycle number but it converges to a certain value as cycle number increases. Figure 5.8 shows the inventory of actinide taken from LWR spent fuel is reduced by a factor of 400 roughly through 100 cycles.

Figure 5.9 shows the mass fraction of cumulative actinide in waste with cycle number. It shows that ^{239}Pu is the most abundant actinide in waste in early cycle but as cycle number increases ^{240}Pu becomes the most abundant actinide in waste. As shown in Table 5.4 ^{239}Pu has the largest fraction and ^{240}Pu has the 2nd largest fraction in the feed material which is taken from LWR spent fuel but as the cycle number increases ^{239}Pu is depleted out due to fission and capture while ^{240}Pu builds up by the neutron capture reaction of ^{239}Pu.

Figure 5.10 shows the cumulative toxicity reduction ratio of actinide with cycle. *The cumulative radiotoxicity reduction ratio is defined as the radiotoxicity of all actinides up to n-th cycle included in the waste stream divided by that of all actinides up to n-th cycle included in the makeup material*. This is a key measure for the transmuting reactor performance in terms of reducing the hazard of actinides. Figure 5.10 shows that the cumulative toxicity of actinides taken from LWR spent fuel is reduced roughly by a factor of 100 through 100 cycle operations.

Figure 5.11 shows the variation of cumulative toxicity fractions of actinides in waste with the cycle number. In early cycles, ^{238}Pu, ^{241}Am, and ^{242}Cm are main sources in toxicity of waste but as cycle number increases the toxicity fraction of ^{241}Am gets smaller instead that of ^{244}Cm increases rapidly and becomes dominant in later cycles. It is noticeable that even though their small mass fractions in waste through entire cycles as shown Figure 5.9, most of toxicity attributes to those isotopes. This is because of their short half-lives and/or relatively small MPC values as shown in Table 4.2. ^{242}Cm isotope builds up rapidly in early cycles from its very small amount contained in the fresh fuel of the startup core and past a peak it decreases slowly until it reaches a steady state. The radioactivity of ^{242}Cm per unit mass is very high compared to other actinides considered in this model due to its very short half-life (163 days). So, even a small increase in the mass of ^{242}Cm isotope can cause a large buildup in its toxicity. ^{244}Cm builds up steadily through entire cycles although its fractional mass in fuel remains small and in later cycles its toxicity becomes most dominant. Its half-life is 18.1 years and MPC value is 3×10^{-11} [Ci/*l*]. Fractional mass of ^{241}Am decreases slowly through entire cycle and so does its fractional toxicity. This implies that the ATW system is able to reduce the toxicity of ^{241}Am very much. Fractional toxicity of ^{238}Pu increases as cycle number increases but due to the effect of a rapid increase in the toxicity of ^{244}Cm it gets decreased in later cycles.

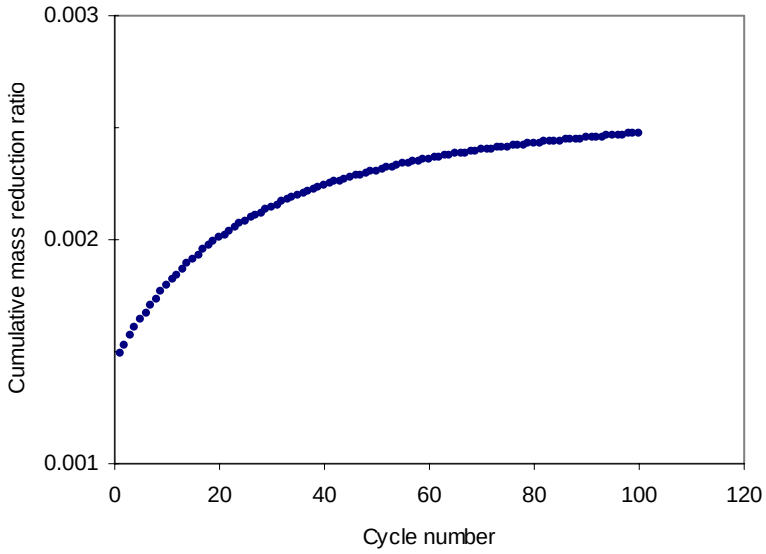

Figure 5.8 Cumulative mass reduction ratio of actinide with cycle number

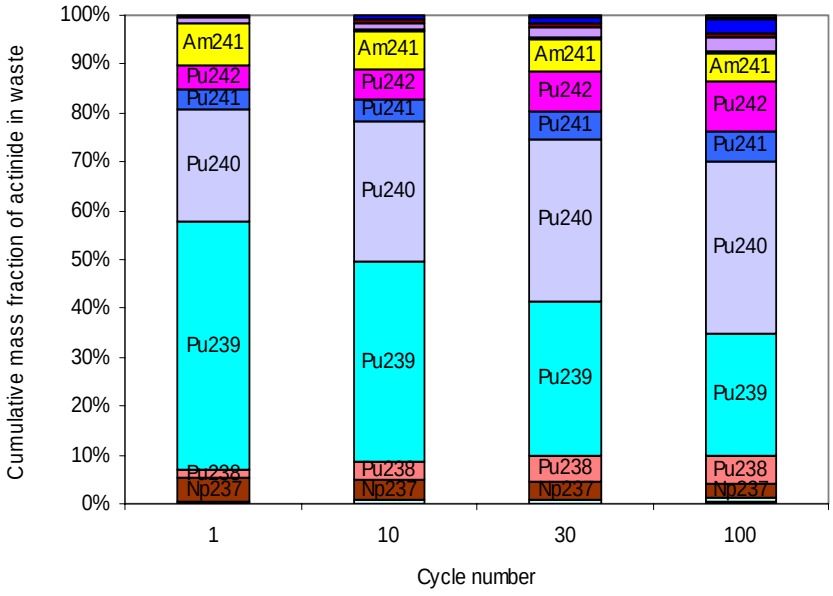

Figure 5.9 Cumulative mass fraction of actinide in waste with cycle number

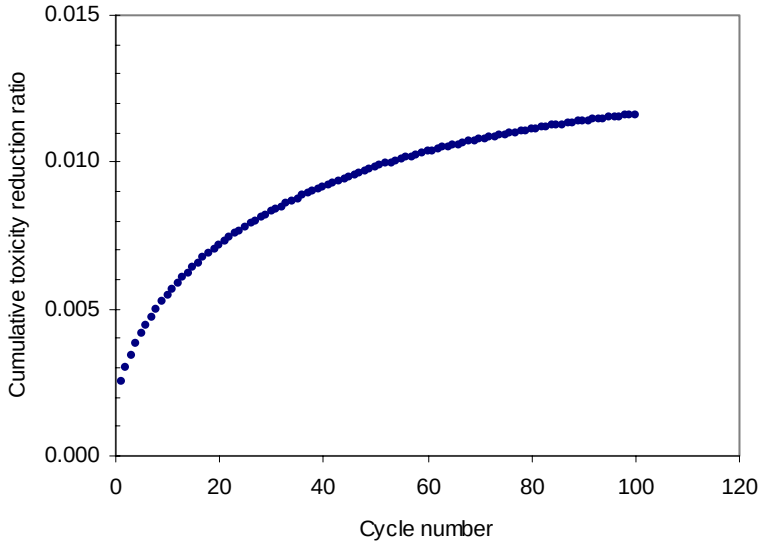

Figure 5.10 Cumulative toxicity reduction ratio of actinide with cycle number

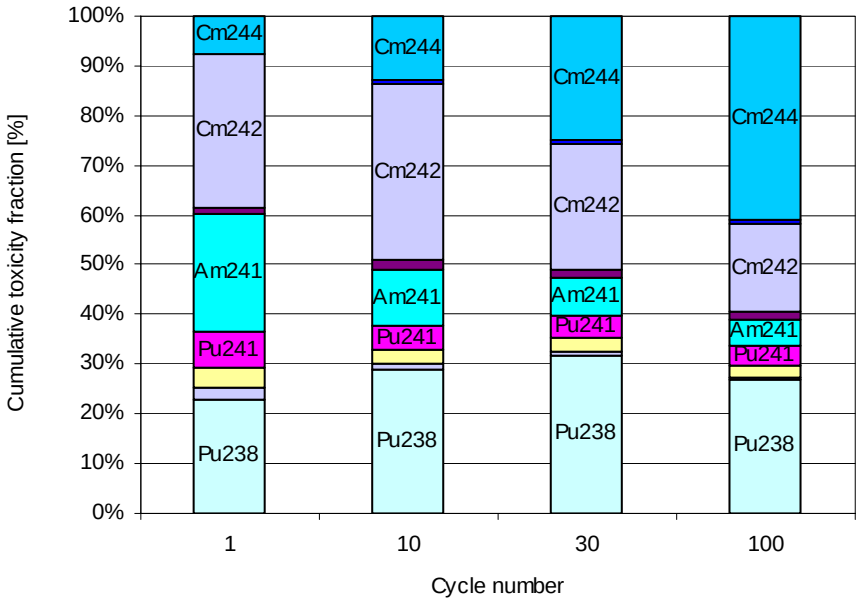

Figure 5.11 Variation of cumulative toxicity fractions of actinides in waste with cycle number

5.4 Effects of Difference in the Branching Ratio of ^{241}Am

In an international benchmark exercise for an accelerator-driven system led by the OECD Nuclear Energy Agency in 1999, noticeable differences have been observed between the calculation results contributed by different organizations [17]. There are many possible reasons for the differences. Among these is the use of different branching ratios for the conversion of ^{241}Am into the two isomers of ^{242}Am. The WACOM code was applied to study the effect of the uncertainty in the branching ratio of ^{242}Am:^{242m}Am on the evolution of the actinides in multi-cycling in an ATW system.

Two sets of branching ratios were considered; one taken from the REBUS3 code system [3] that used the branching ratio of 0.80 to 0.20 for ^{242}Am to ^{242m}Am whereas the other from ORIHET3 [18], an adaptation of the ORIGEN code, that used 0.85 to 0.15 for the branching ratio. Figure 5.12 shows the simplified transmutation chain of Am isotopes used in WACOM. Neutron reactions of ^{242}Am and ^{244}Am which have very short half-lives (16h, 10h) are neglected and they are assumed to decay into their daughters instantaneously.

Table 5.6 shows the WACOM results for the actinide composition in the fuel after a single irradiation cycle. The relative difference in concentration caused by use of different branching ratios is the largest for ^{242m}Am followed by ^{242}Cm and ^{243}Cm. The branching ratio difference has only a very small effect on the concentration of the other isotopes. However, this effect increases with the cycle number, as shown in Table 5.7.

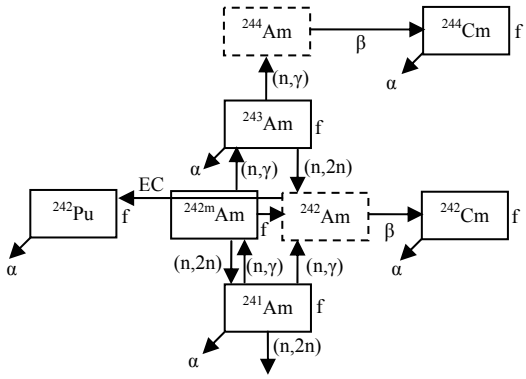

Figure 5.12 Transmutation chain of Am-isotopes used in WACOM

Table 5.6 Actinide Compositions in Fuel after a Single Cycle Irradiation

Isotope	^{242}Am:^{242m}Am (0.8:0.2)	^{242}Am:^{242m}Am (0.85:0.15)	Relative Difference
U234	8.781E+22	8.795E+22	-0.16%
U235	1.349E+23	1.349E+23	0.01%
U236	8.821E+22	8.822E+22	-0.01%
U238	1.595E+25	1.595E+25	0.00%
Np237	1.568E+26	1.568E+26	0.01%
Pu238	5.377E+25	5.393E+25	-0.30%
Pu239	1.615E+27	1.615E+27	0.01%
Pu240	7.373E+26	7.373E+26	0.00%
Pu241	1.259E+26	1.259E+26	0.00%
Pu242	1.573E+26	1.575E+26	-0.13%
Am241	2.757E+26	2.757E+26	0.01%
Am242m	4.610E+24	3.555E+24	22.90%
Am243	3.186E+25	3.186E+25	0.02%
Cm242	1.294E+25	1.376E+25	-6.35%
Cm243	1.700E+23	1.773E+23	-4.28%
Cm244	5.421E+24	5.423E+24	-0.03%
Cm245	4.342E+23	4.343E+23	-0.04%
Cm246	3.749E+22	3.750E+22	-0.02%

Table 5.7 Actinide Compositions in Fuel after 100 Cycle Irradiation

Isotope	^{242}Am:^{242m}Am (0.8:0.2)	^{242}Am:^{242m}Am (0.85:0.15)	Relative Difference
U234	1.322E+25	1.370E+25	-3.63%
U235	3.497E+24	3.611E+24	-3.28%
U236	5.329E+24	5.433E+24	-1.95%
U238	5.772E+25	5.788E+25	-0.28%
Np237	1.249E+26	1.252E+26	-0.30%

Pu238	2.716E+26	2.808E+26	-3.39%
Pu239	1.093E+27	1.098E+27	-0.46%
Pu240	1.752E+27	1.756E+27	-0.21%
Pu241	3.125E+26	3.127E+26	-0.08%
Pu242	5.692E+26	5.752E+26	-1.06%
Am241	2.610E+26	2.618E+26	-0.30%
Am242m	2.028E+25	1.528E+25	24.66%
Am243	1.818E+26	1.822E+26	-0.22%
Cm242	3.007E+25	3.193E+25	-6.19%
Cm243	2.980E+24	3.155E+24	-5.86%
Cm244	1.718E+26	1.719E+26	-0.04%
Cm245	5.159E+25	5.157E+25	0.04%
Cm246	2.662E+25	2.652E+25	0.38%

5.5 Summary and Conclusions

A modification has been implemented to WACOM model developed for efficient simulation of the evolution of the fuel and waste composition and inventory in ATW systems. To account for the variation in the neutron spectrum of a transmuting reactor core a simple strategy has been implemented to the developed code. This strategy involves interpolation of effective one-group cross sections generated with MCNP for the start up core composition and an equilibrium core composition. A linear interpolation scheme was found to be adequate; it enables prediction of the fuel composition evolution while satisfying the k_{eff} constraint using only two MCNP calculations.

It is estimated that the mass fraction of actinides of BOC-fuel in a LBE cooled transmuting reactor increases from ~32% to ~41%, if the k_{eff} control is achieved by adjusting the actinides-to-zirconium volume ratio. The corresponding cycle duration increases from ~86 days to ~144 days. The variation in the actinides weight percent and in the cycle duration are particularly pronounced during the first 20 cycles and taper off after

~60 cycles. The mass of actinide in the LWR spent fuel is reduced by a factor of ~400 and the toxicity of actinide in the LWR spent fuel is reduced by a factor of ~100.

Effects of difference in the branching ratio of ^{241}Am on results of multi-cycle analyses for the ATW reactor have also been investigated. It is found that a 5% difference in the branching ratios of ^{241}Am makes a significant difference in the ^{242m}Am concentration and some differences in the ^{242}Cm and ^{243}Cm concentrations after a single irradiation cycle. After 100 cycles the discrepancy propagates to other radionuclides such as U and Pu isotopes. These findings indicate that accurate estimation of the branching ratio of ^{241}Am is important for reliable evaluations of actinide transmutation performance.

6 Reduction of TRU Toxicity in LWR Spent Fuel

6.1 Introduction

In Chapter 5, we dealt with a modification of WACOM to take into account the variation in the neutron spectrum of a transmuter core and it is found that the implemented linear interpolating scheme enables the prediction of the time- and cycle- dependent evolution of fuel isotopes in the transmuter core adequately. In this Chapter, to investigate the reduction of TRU toxicity in LWR-SNF, the reference LBE-cooled transmuter which has been analyzed by modified WACOM in Chapter 5 is applied to the reference ATW plant illustrated in Figure 1.2. The reference ATW plant is assumed to employ eight of the LBE-cooled subcritical transmuters to process a specific amount of LWR-SNF (10,155 MT). Most of TRU taken from 10,155 MT of LWR-SNF is transmuted into fission products while generating electricity by the reference ATW plant. According to the deployment scenario described in [2], 8.5 reference ATW plants are supposed to be in operation in a staggered manner to process 86,317 MT of LWR-SNF.

The mass and the composition of the TRU from the waste streams of the entire operation of the reference ATW plants are estimated and then compared with those of the TRU originally included in the LWR-SNF in the aspects of mass and toxicity reductions. Transmutations of long-lived fission products such as Tc and I are not treated here even though the reference ATW plant aims to the reduction of those as well.

6.2 Reference ATW Plant Sized to Process 10,155 MT of LWR-SNF

In the reference ATW plant illustrated in Figure 1.2, the separations process includes three steps. The uranium is first removed via the UREX process and then by an oxide-reduction process, transuranics and fission products are converted from oxide to metallic form. Finally the transuranic components are separated and converted into ATW fuel. 99.9% of the TRU and 95% of Tc and I in SNF are supposed to be separated from uranium and other fission products. Through separations process, 355 MT of stable or short-lived fission products, 0.43 MT of ^{99}Tc, 0.12 MT of ^{127}I & ^{129}I , and 0.11 MT of TRU comes from waste stream while 9,684 MT of uranium, 106 MT of TRU, 2.3 MT of iodine, and 8.1 MT of technetium are recovered. Among materials recovered, TRU, iodine, and technetium are fabricated into blankets of ATW transmuters for transmutation. The remaining uranium could be disposed of as low-level waste or recycled.

The reference ATW plant is sized to produce a net power of 6,720 MWt by fissioning 1.767 MT TRU per year. It has eight subcritical transmuters and thus each transmuter will process 1/8 of 1.767 MT TRU per year. During the 60-year plant life time, an ATW plant is supposed to consume ~106 MT of TRU.

Figure 6.1 shows the reference ATW plant implementation scenario. Around 2030, an ATW power plant which is a prototype and has four subcritical transmuters would begin operating and will process about 5,000 MT of SNF. The full deployment of an eight-unit ATW system could then proceed.

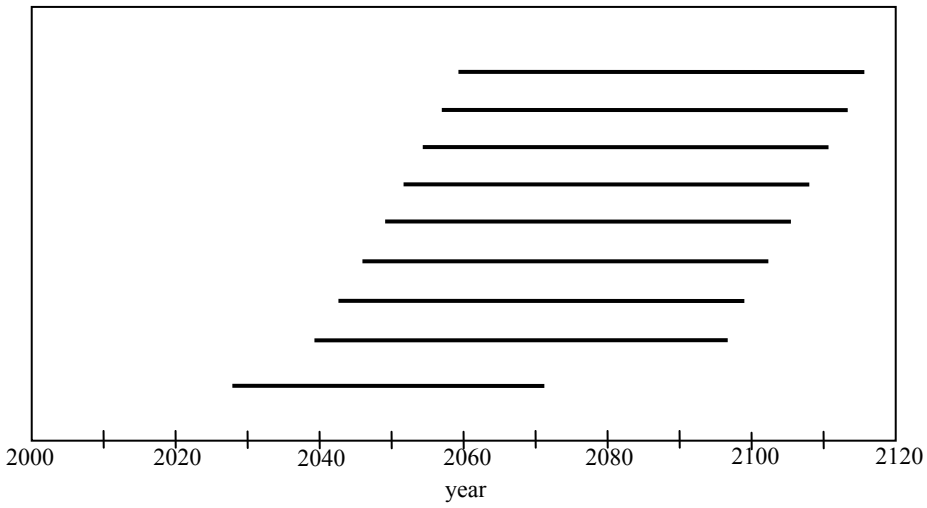

Figure 6.1 Reference ATW plant implementation to address the 86,317 MT of spent fuel [2]

Reference ATW plant parameters used in the roadmap for the separation facility, the accelerator, and the transmuter systems are summarized in Tables 6.1 through Table 6.3.

Table 6.1 Reference ATW Plant Parameters for the Separation Facility [2]

TRU loss fraction per pass	0.001
Total processing loss	0.0033
Tc & I processing loss	0.05
TRU Throughput	1765.8 kg/yr
^{99}Tc Throughput	135.6 kg/yr
I Throughput	37.9 kg/yr
Spent Fuel Throughput	169.2 tn/yr

Table 6.2 Reference ATW Plant Parameters for the Accelerator [2]

Proton energy	1 GeV
Proton current	90 mA
Number of beam lines	2
Beam power	90.0 MW
Power required-accelerator	304.0 MWe
Accelerator net efficiency	29.6 %
Power required-plant	378.6 MWe

Table 6.3 Reference ATW Plant Parameters for the Transmuter Systems [2]

k_{eff}	0.97
ν (neutrons/fission)	2.95
Energy per fission	208 MeV

Thermodynamic efficiency	37.0%
Plant capacity factor	70.0%
Fission/socond/target	2.5E+19
Fission/year/target	5.52E+26
kg TRU fissioned/year/target	220 kg TRU/yr
Tc conversion efficiency	0.7
I conversion efficiency	0.7
Fission heat	832.1 MWt
Target/blanket total heat	840.0 MWt
Electricity per target/blanket	310.8 Mwe
Net plant efficieny	31.4 %

6.3 Characteristics of the Reference LBE-Cooled Subcritical Transmuter

In section 6.2, the key features of the reference ATW plant and its deployment scenario were overviewed and its parameters are listed in tables. In this section, we replace the ATW parameters for the transmuter systems shown in Table 6.3 with the parameters for the reference LBE-cooled transmuter, which were estimated by modified WACOM in Chapter 5.

It is found that the LBE-cooled transmuter in an equilibrium cycle consumes 0.246 MT TRU obtained from SNF per year to produce the power of 840 MWt. This amount is a little larger than that shown in Table 6.3. The difference mainly arises because the LBE-cooled transmuter in the present study is assumed to produce a power of 840 MWt by fissioning TRU only, whereas in the Roadmap the power of 840 MWt is assumed to be generated from both fission of TRU blanket (832.1 MWt) and target spallation (7.9 MWt). In addition, in the Roadmap the average recoverable energy per fission is assumed to be 208 MeV for any TRU isotopes, whereas in this calculation each TRU isotope is assumed to have a value as shown in Table 4.2. This difference in TRU consumption rates, however, does not affect

on the amount of TRU waste produced from the reference ATW plant operation, but affects on the plant operating period required to consume the 900 MT TRU.

Thus, 8.5 reference ATW plants containing 68 transmuters treat 16.73 MT TRU per year, resulting in 54 years to process 900 MT TRU instead of 60 years. With cycle-by-cycle analyses, we have also figured out that it takes 56 years for 68 transmuters to consume 900 MT TRU. Cycle duration for the equilibrium cycle was estimated to be ~144 days. About 60 cycles (30 years) are required for a LBE-cooled transmuter to reach an equilibrium and during this period ~52% of TRU is fissioned. The performance characteristics of the LBE-cooled transmuter estimated by WACOM are listed in Table 6.4.

Table 6.4 Performance Characteristics of the Reference LBE-Cooled Transmuter Estimated by WACOM

Multiplication factor	BOEC[1]	0.980
	EOEC[2]	0.920
Burnup reactivity loss (%Δk)		6.1
Equilibrium % TRU fissioned		27.2
Equilibrium TRU waste from ATW fuel separation process (kg/year)		0.659
Equilibrium TRU consumption rate (kg/year)		246
Equilibrium loading (kg/year)	LWR-TRU	246
	Recycled-TRU	658
	Total TRU	904
TRU inventory (kg)	BOEC	2100
	EOEC	1977
Fission products inventory (kg)	BOEC	617
	EOEC	740
Zirconium inventory (kg)	BOEC	2398
	EOEC	2398

[1] Beginning of equilibrium cycle
[2] End of equilibrium cycle

6.4 Reduction of TRU by the Reference ATW Plant with LBE-Cooled Transmuters

After a successful operation of the reference ATW plant, the total mass of TRU, which would be included in the waste stream is quantified to be 5.291 MT. It comes from three sources: (1) 0.935 MT TRU included in the waste arising from reprocessing of 86,317 MT SNF, (2) 2.380 MT TRU included in the waste from ATW fuel processing in a 56-year operation period (estimated by cycle by cycle analysis instead of equilibrium analysis), and (3) 1.976 MT TRU included in the last LBE transmuter core. For (1) and (2), composition change of TRU included in the waste stream by radioactive decay during the ATW operating period was not taken into account and for (3), it is assumed that any residual quantities of TRU remaining in the plant shut down would be fed into any ATW plants that remain in operating mode. The isotopic composition of (1) is supposed to be the same with that of LWR-TRU because the same recovery fraction was applied for all LWR-TRU isotopes in LWR-spent fuel separation process. The isotopic compositions of (2) and (3) are quite different from that of (1). By recycling of TRU during the ATW plant operation period, the fractional mass of Pu239 which is the most abundant isotope in LWR-TRU decreases from ~53% to ~24% in ATW-TRU waste, while that of Pu240 increases from ~22% to ~35%. It is noticeable that the separation waste from ATW fuel reprocessing is much more than that from LWR-SNF reprocessing. The difference comes because the former gets to pass through the ATW fuel processing facility many times due to TRU-recycling in ATW fuel cycle. The isotopic compositions of three different TRU waste sources are shown in Table 6.5.

Thus, original 900 MT TRU in SNF has been reduced to 5.291 MT (i.e., by a factor of 170) by the assumed ATW system deployment scenario. Table 6.6 shows the mass reduction factor of each TRU isotope, which is defined as the ratio of the mass of an isotope in 900 MT TRU to that in 5.291 MT TRU. The isotopic composition of 5.291 MT TRU represents a sum of three-TRU waste sources described in the previous paragraph. This table shows that Np-237, Pu-239, Pu-240, Pu-241, and Am-241 can be reduced more than a factor of one hundred by the reference ATW plant employing LBE-cooled subcritical transmuters. Table 6.6 also shows that the factor is greater than the overall mass reduction factor, 170, for Pu-239, Np-237, and Am-241, which means that reduction of these isotopes could be done preferentially.

Table 6.5 Isotopic Compositions of 0.935 MT, 2.380 MT, and 1.976 MT TRU

Isotope	0.935 MT TRU[3] [wt%]	2.380 MT TRU [wt%]	1.976 MT TRU [wt%]
U234	0.000	0.224	0.260
U235	0.004	0.057	0.069
U236	0.002	0.072	0.106
U238	0.478	0.987	1.155
Np237	5.023	2.731	2.487
Pu238	1.272	5.546	5.420
Pu239	53.196	24.454	21.986
Pu240	21.534	35.168	35.360
Pu241	3.782	6.261	6.332
Pu242	4.686	10.546	11.601
Am241	8.967	5.630	5.268
Am242m	0.014	0.429	0.413
Am243	0.926	3.244	3.718
Cm242	0.000	0.660	0.613
Cm243	0.002	0.064	0.061
Cm244	0.104	2.819	3.526
Cm245	0.009	0.803	1.064
Cm246	0.001	0.320	0.552

[3] 33,000 MWd/MT burnup PWR spent fuel with 25-year cooling time (99.995% of the uranium is removed in the UREX process) [12]

Table 6.6 Mass Reduction Factor of Each TRU-Isotope by the Reference ATW Plant

Isotope	900 MT TRU [#]	5.291 MT TRU [#]	Mass reduction factor
U234	6.70E+17	2.67E+25	2.51E-08
U235	9.25E+25	6.98E+24	1.33E+01
U236	4.60E+25	9.78E+24	4.71E+00
U238	1.09E+28	1.28E+26	8.49E+01
Np237	1.15E+29	4.10E+26	2.81E+02
Pu238	2.90E+28	6.33E+26	4.59E+01
Pu239	1.21E+30	3.82E+27	3.17E+02
Pu240	4.87E+29	4.34E+27	1.12E+02
Pu241	8.53E+28	7.71E+26	1.11E+02
Pu242	1.05E+29	1.30E+27	8.11E+01
Am241	2.02E+29	8.05E+26	2.51E+02
Am242m	3.14E+26	4.58E+25	6.86E+00
Am243	2.07E+28	3.92E+26	5.28E+01
Cm242	1.97E+18	6.90E+25	2.86E-08
Cm243	4.47E+25	6.77E+24	6.60E+00
Cm244	2.32E+27	3.37E+26	6.87E+00
Cm245	2.00E+26	9.79E+25	2.04E+00
Cm246	2.21E+25	4.62E+25	4.78E-01

For Np-237 and its precursor, Am-241, which are considered the main source of radiological hazards in a long-term period in a geological repository, their mass reduction factors are 281 and 251 (Table 6.6), respectively. This implies that we could reduce radiological impacts from those isotopes on a geological repository significantly by the reference ATW plant operation.

Table 6.7 Radiotoxicity Reduction Factor of Each TRU-Isotope by the Reference ATW Plant

Isotope	900 MT TRU [*l*]	5.291 MT TRU [*l*]	Radiotoxicity reduction factor
U234	5.42E+03	2.16E+11	2.51E-08
U235	2.60E+08	1.96E+07	1.33E+01
U236	3.89E+09	8.26E+08	4.71E+00
U238	4.83E+09	5.69E+07	8.49E+01
Np237	1.59E+15	5.67E+12	2.81E+02
Pu238	9.83E+18	2.14E+17	4.59E+01
Pu239	1.49E+18	4.70E+15	3.17E+02
Pu240	2.21E+18	1.96E+16	1.12E+02
Pu241	3.84E+18	3.47E+16	1.11E+02

Pu242	8.35E+15	1.03E+14	8.11E+01
Am241	1.39E+19	5.52E+16	2.51E+02
Am242m	6.62E+16	9.65E+15	6.86E+00
Am243	8.34E+16	1.58E+15	5.28E+01
Cm242	3.75E+09	1.31E+17	2.86E-08
Cm243	2.95E+16	4.47E+15	6.61E+00
Cm244	2.53E+18	3.69E+17	6.87E+00
Cm245	6.97E+14	3.42E+14	2.04E+00
Cm246	1.38E+14	2.88E+14	4.78E-01
Total	3.40E+19	8.45E+17	4.02E+01

Table 6.7 shows the radiotoxicity of each TRU isotope in 900 MT TRU and in 5.291 MT TRU, and the radiotoxicity reduction factor of each isotope, which is defined as the ratio of the radiotoxicity of an isotope in 900 MT TRU to that in 5.291 MT TRU is listed in the last column. The radiotoxicity reduction factor of each TRU isotope has the same value with the mass reduction factor of each TRU isotope as shown in Table 6.6 because the radiotoxicity of an isotope is directly proportional to its mass. However, the overall radiotoxicity reduction factor is much less than the overall mass reduction factor because the mass fraction of Cm-isotopes is greater in ATW-TRU (~4.2 %) than in SNF-TRU (~0.1 %) and maximum permissible concentrations (MPC) of Cm-isotopes in water are relatively small. Figures 6.3 and 6.4 show the mass fraction and the radiotoxicity fraction of each TRU isotope in 900 MT TRU and in 5.291 MT TRU, respectively. In both 900 MT TRU and 5.291 MT TRU, the mass fraction of Pu is dominant but the most abundant isotope in 900 MT TRU is Pu239, whereas in 5.291 MT TRU is Pu-240. In radiotoxicity fraction, that of Pu-isotopes is dominant in 900 MT TRU while that of Cm-isotopes in 5.291 MT TRU. The radiotoxicity fraction of Cm-isotopes in 5.291 MT TRU is ~60% while in 900 MT TRU it is ~8%.

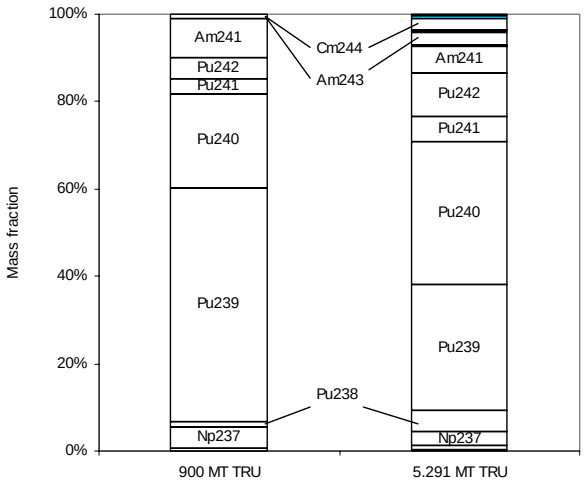

Figure 6.3 Mass fraction of TRU isotopes in 900 MT TRU and 5.291 MT TRU

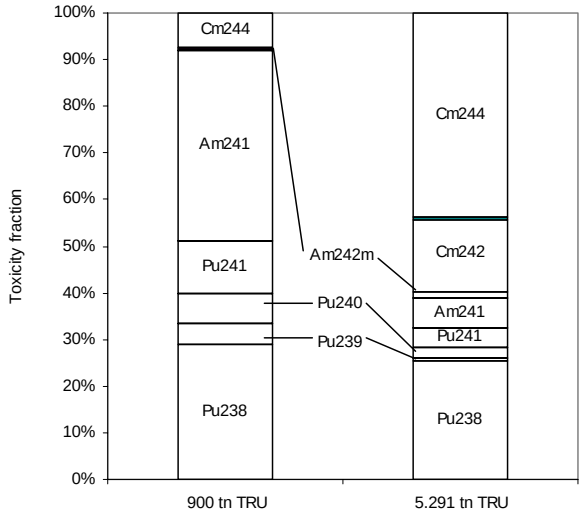

Figure 6.4 Toxicity fraction of TRU isotope in 900 MT TRU and 5.291 MT TRU

Figure 6.5 shows the variation of radiotoxicity reduction factor with time after waste generation. It represents that how the radiotoxicity ratio of a TRU isotope in 900 MT TRU to that in 5.291 MT TRU evolves with time. In the early-time domain, the total radiotoxicity reduction factor is as small as 40 at 0.1 year because the fractional

radiotoxicity of Cm-isotopes (^{242}Cm, ^{244}Cm) are significant in ATW-TRU as shown in Figure 6.4. However, most of Cm-242 and Cm-244 isotopes decay out within 100 years and thus the factor increases up to 100. This also implies that if the cooling time of ATW-TRU is taken into account in a more realistic manner in the model, the total rediotoxicity reduction factor in early-time domain would be much larger than 40.

Figure 6.5 also shows that the radiotoxicity reduction factor of Np-237 decreases from 280 to 200 in a time period between ~10 year and ~10,000 years. In this time period, most of Pu-241 decays into Am-241, and then into Np-237 in both 900 MT TRU and 5.291 MT TRU because the radiotoxicity reduction factors of Am-241 and Pu-241 are smaller than that of Np-237. After 10,000 years, the radiotoxicity reduction factor of Np-237 remains constant.

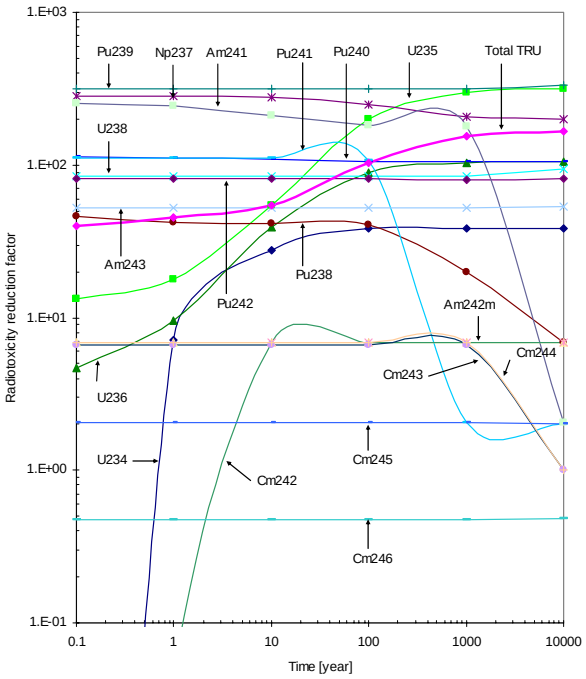

Figure 6.5 Variation of radiotoxicity reduction factor with time after waste generation.

6.5 Discussions

In this chapter, we have estimated the reduction of TRU waste based on the reference ATW plant implementation scenario. The result shows that the reduction of TRU mass seems to be much less than the prediction (by factor of ~1000) made in the Roadmap. Among three TRU waste sources, TRU waste from ATW fuel processing was not estimated explicitly in the Roadmap as shown in Figure 1.2. According to the analysis of the ATW fuel cycle performed in [ ], however, the amount of TRU waste which would be included in ATW separation waste is not negligible. It could be a major TRU waste source as estimated in section 6.4. Of course, the amount of TRU waste from ATW fuel processing could change if a different operating mode is applied for the performance analysis of the ATW fuel cycle. For an example, the recovery fraction of TRU assumed in ATW fuel processing will be one of key parameters to the determination of the amount of TRU waste. However, for any case, it seems that certain amount of TRU waste from ATW fuel separation process would be unavoidable.

The amount of TRU waste from the last transmuter could also be changed. Even though we assume that its operating is controlled by the reactivity constraint, it could be possible to allow more burnup for the last transmuter in its final operating cycle for the purpose of destructing TRU remaining in the core. It is also possible to modify the core design, make it thermal or close to thermal, and thereby significantly reduce the TRU inventory needed for getting k_{eff} of ~0.98. By doing so, we could reduce to some extent, but not completely, the amount of TRU waste from the decommissioning of the last transmuter.

For the estimation of the reduction of the radiotoxicity of LWR-TRU, as mentioned in section 6.4, by considering cooling time of ATW spent fuel before and during separation process, cooling time of TRU waste cumulated in waste stream, and the time required for refueling in each cycle it could be possible to get a greater reduction factor at the end of the reference ATW plant operation. However, in spite of the small radiotoxicity reduction factor in early time domain due to aforementioned assumptions, we could get a profile describing a time-dependent variation of the radiotoxicity reduction factor and in long-term period it provides us how much the radiological hazard of Np-237 could be reduced by the reference ATW plant implementation.

6.6 Conclusion

In this study, we have investigated the performance of a reference ATW plant employing LBE-cooled subcritical transmuters as its transmuters.

Estimated ATW-TRU waste was 5.291 MT through the reference ATW system. But it should be noticed that the result shown here is a “snapshot” of one possible case among infinitely many. If we use different operating conditions and make assumptions more realistically, the amount of ATW-TRU waste and its composition could be different from the results obtained here.

In an aspect of TRU reduction, the results show that the mass of LWR-TRU can be reduced more than a factor of 170 and the radiotoxicity can be decreased more than a factor of 40 at the end of the reference ATW plant operation. After ~1000 years, the overall

radiotoxicity reduction factor increases up to ~156 because most of Cm-isotopes included in ATW-TRU waste decay out within that time period.

The radiotoxicity reduction factor was greater than the overall mass reduction factor, 170, for Pu-239, Np-237, and Am-241, which means that reduction of these isotopes could be done preferentially. This implies that the ATW deployment can decrease not only the radiotoxicity of TRU isotopes but also long-lived radionuclides, such as Np237, which determine radiological impact of the repository in a preferential manner, compared to other TRU isotopes. After a successful operation of the reference ATW plant, both the inventory and the radiotoxicity of Np-237 in LWR-TRU could be reduced by a factor of 281. In long-term analysis, the radiotoxicity reduction factor of Np-237 decreases due to the decay of its precursor until the inventory of its precursor becomes negligibly small. In 1,000 years its value decreases up to 206 and after 10,000 years it almost remains constant as ~200.

REFERENCES

[1] DOE/RW-0519, "A Roadmap for Developing ATW Technology- A Report to Congress," October 1999.

[2] D. Hill, *et al*., "A Roadmap for Developing ATW Technology: Systems Scenarios & Integration", ANL/RE-99/16, September 1999.

[3] B. J. Toppel, "A User's Guide for the REBUS-3 Fuel-Cycle-Analysis Capability", ANL-83-2, Argonne National Laboratory, (1983).

[4] R. L. Moore, B. G. Schnitzler, C. A. Wemple, R. S. Babcock, and D. E. Wessol, "MOCUP: MCNP- ORIGEN2 Coupled Utility Program", Idaho National Engineering Laboratory, (1995).

[5] D. L. Poston and H. R. Trellue, "User's Manual, Version 2.0 for MONTEBURNS Version1.0," "LA-UR-99-4999, September 1999.

[6] RSICC Code Package CCC-371, "ORIGEN 2.1-Isotope Generation and Depletion Code Matrix Exponential Method", (1999).

[7] RSICC Code Package CCC-700, "MCNP4C, Monte Carlo N-Particle Transport Code System", April 2000.

[8] Nuclear Data Evaluation Lab., Korea Atomic Energy Research Institute: "Table of the Nuclides", http://atom.kaeri.re.kr, (2000).

[9] A. G. Croff, "ORIGEN2: A Versatile Computer Code for Calculating the Nuclide Compositions and Characteristics of Nuclear Materials", *Nuclear Technology*, **Vol. 62**, September 1983.

[10] J. J. Duderstadt, L. J. Hamilton, "Nuclear Reactor Analysis," John Wiley & Sons, Inc. (1976)

[11] S. C. Chapra and R.P. Canale, "*Numerical Methods for Engineers*", McGraw-Hill, (1998).

[12] AAA-RPO-SYS-01-0008, LA-UR-01-1817, "Compendium of Initial System Point Designs for Accelerator Transmutation of Radioactive Waste", February 2001.

[13] U.S. Nuclear Regulatory Commission, NRC regulations (10CFR): "Appendix B", http://www.nrc.gov/reading-rm/doc-collections/cfr/part020, (2002).

[14] Bruce W. Spencer, "The Rush to Heavy Metal Reactor Coolants-Gimmick or Reasoned", *Proc. 8th Intl. Conf. on Nuclear Engineering*, ICONE8, Baltimore, MD, USA, April 2-6, 2000.

[15] "*Liquid Material Handbook*", 23rd ed., the Atomic Energy Commission, Department of Navy, Washington, D.C., (1952).

[16] IAEA-TECDOC-1039, "Influence of High Dose Irradiation on Core Structural and Fuel Materials in Advanced Reactors", June 1997.

[17] NEA/NSC/DOC(2001)13, "Comparison Calculations for an Accelerator-Driven Minor Actinide Burner", (2001).

[18] F. Atchison and H. Schaal, "ORIHET3-Version 1.12 A Guide for Users," March, 2001